NAVAL POSTGRADUATE SCHOOL

MONTEREY, CALIFORNIA

THESIS

LOW-COST, DISPOSABLE MEMS RADIATION DETECTORS USING GAMMA-SENSITIVE POLYMERS

by

Benjamin P. McHale

June 2020

Thesis Advisor:	Dragoslav Grbovic
Co-Advisor:	Claudia C. Luhrs
Second Reader:	Craig F. Smith

Approved for public release. Distribution is unlimited.

THIS PAGE INTENTIONALLY LEFT BLANK

REPORT DOCUMENTATION PAGE	*Form Approved OMB No. 0704-0188*

Public reporting burden for this collection of information is estimated to average 1 hour per response, including the time for reviewing instruction, searching existing data sources, gathering and maintaining the data needed, and completing and reviewing the collection of information. Send comments regarding this burden estimate or any other aspect of this collection of information, including suggestions for reducing this burden, to Washington headquarters Services, Directorate for Information Operations and Reports, 1215 Jefferson Davis Highway, Suite 1204, Arlington, VA 22202-4302, and to the Office of Management and Budget, Paperwork Reduction Project (0704-0188) Washington, DC 20503.

1. AGENCY USE ONLY *(Leave blank)*	**2. REPORT DATE** June 2020	**3. REPORT TYPE AND DATES COVERED** Master's thesis

4. TITLE AND SUBTITLE LOW-COST, DISPOSABLE MEMS RADIATION DETECTORS USING GAMMA-SENSITIVE POLYMERS	**5. FUNDING NUMBERS**
6. AUTHOR(S) Benjamin P. McHale	
7. PERFORMING ORGANIZATION NAME(S) AND ADDRESS(ES) Naval Postgraduate School Monterey, CA 93943-5000	**8. PERFORMING ORGANIZATION REPORT NUMBER**
9. SPONSORING / MONITORING AGENCY NAME(S) AND ADDRESS(ES) DTRA	**10. SPONSORING / MONITORING AGENCY REPORT NUMBER**

11. SUPPLEMENTARY NOTES The views expressed in this thesis are those of the author and do not reflect the official policy or position of the Department of Defense or the U.S. Government.

12a. DISTRIBUTION / AVAILABILITY STATEMENT Approved for public release. Distribution is unlimited.	**12b. DISTRIBUTION CODE** A

13. ABSTRACT (maximum 200 words)

Micro-electrical mechanical systems (MEMS) radiation detectors can be used in a variety of fields, such as medicine, homeland security, and the nuclear power industry, and for a variety of applications, such as environmental studies and mining and geologic characterization. The objective of this thesis was to quantify the effect of gamma radiation on the gamma-sensitive polyvinylidene difluoride (PVDF) dielectric. These gamma-sensitive detectors produce real-time results and, due to their small size and low cost, can be implemented on a larger scale than traditional radiation-detection methods. It was hypothesized that the gamma radiation would increase the dielectric constant and thus the capacitance of the dielectric. Copper plates, acrylic plates, and aluminum foil were used in this research. The study concluded that the gamma radiation did increase the dielectric constant of the PVDF dielectric. However, environmental factors such as temperature, humidity, and light exposure appeared to have a concurrent effect on the dielectric constant.

14. SUBJECT TERMS capacitor, micro-electrical mechanical systems, MEMS, radiation, detector, polymer, polyvinylidene difluoride, PVDF	**15. NUMBER OF PAGES** 99
	16. PRICE CODE

17. SECURITY CLASSIFICATION OF REPORT	**18. SECURITY CLASSIFICATION OF THIS PAGE**	**19. SECURITY CLASSIFICATION OF ABSTRACT**	**20. LIMITATION OF ABSTRACT**
Unclassified	Unclassified	Unclassified	UU

NSN 7540-01-280-5500 Standard Form 298 (Rev. 2-89) Prescribed by ANSI Std. 239-18

THIS PAGE INTENTIONALLY LEFT BLANK

Approved for public release. Distribution is unlimited.

LOW-COST, DISPOSABLE MEMS RADIATION DETECTORS USING GAMMA-SENSITIVE POLYMERS

Benjamin P. McHale
Ensign, United States Navy
BS, United States Naval Academy, 2019

Submitted in partial fulfillment of the
requirements for the degree of

MASTER OF SCIENCE IN MECHANICAL ENGINEERING

from the

NAVAL POSTGRADUATE SCHOOL
June 2020

Approved by: Dragoslav Grbovic
Advisor

Claudia C. Luhrs
Co-Advisor

Craig F. Smith
Second Reader

Garth V. Hobson
Chair, Department of Mechanical and Aerospace Engineering

THIS PAGE INTENTIONALLY LEFT BLANK

ABSTRACT

Micro-electrical mechanical systems (MEMS) radiation detectors can be used in a variety of fields, such as medicine, homeland security, and the nuclear power industry, and for a variety of applications, such as environmental studies and mining and geologic characterization. The objective of this thesis was to quantify the effect of gamma radiation on the gamma-sensitive polyvinylidene difluoride (PVDF) dielectric. These gamma-sensitive detectors produce real-time results and, due to their small size and low cost, can be implemented on a larger scale than traditional radiation-detection methods. It was hypothesized that the gamma radiation would increase the dielectric constant and thus the capacitance of the dielectric. Copper plates, acrylic plates, and aluminum foil were used in this research. The study concluded that the gamma radiation did increase the dielectric constant of the PVDF dielectric. However, environmental factors such as temperature, humidity, and light exposure appeared to have a concurrent effect on the dielectric constant.

THIS PAGE INTENTIONALLY LEFT BLANK

TABLE OF CONTENTS

LIST OF FIGURES

THIS PAGE INTENTIONALLY LEFT BLANK

LIST OF TABLES

THIS PAGE INTENTIONALLY LEFT BLANK

LIST OF ACRONYMS AND ABBREVIATIONS

Cs-137	Cesium 137
MEMS	Micro-electrical mechanical systems
MRI	Magnetic resonance imaging
NMP	N-Methyl-2-pyrrolidone
PVDF	Polyvinylidene difluoride
TLD	Thermoluminescent detector
Z	Atomic number

THIS PAGE INTENTIONALLY LEFT BLANK

ACKNOWLEDGMENTS

I would like to express my sincerest gratitude to several NPS faculty members for their unconditional support. My thesis advisors, Dr. Grbovic and Dr. Smith, placed their trust in me to complete my research. I went through several iterations of experiments, and their guidance and expertise were essential moving forward. Dr. Luhrs from the Mechanical and Aerospace Engineering Department was crucial to the success of my research as well. She helped secure lab spaces and materials necessary for me to conduct my experiments. Lastly, I would like to thank my father, Paul McHale, for his unwavering support. He serves as an inspiration for me in my naval career.

THIS PAGE INTENTIONALLY LEFT BLANK

I. INTRODUCTION

Ionizing radiation has always been a part of the human environment. However, it was not until around 100 years ago that instruments were used to detect this phenomenon. Ionizing radiation refers to energy that "travels in the form of electromagnetic waves (gamma or X-rays) or particles (neutrons, beta, or alpha)" [1]. X-rays were discovered on November 8, 1895, when "Rontgen noticed that a piece of cardboard coated with barium platinocyanide showed a faint, flickering, greenish light (fluorescence) when electrical discharges took place in a Hittorf-Crookes tube near the screen" [2]. Following this discovery, Rontgen made the first medical X-ray photograph on December 22, 1895. This marked the beginning of radiation detection. In 1896, Henri Becquerel took this experiment further discovering radioactivity emanating from uranium minerals [2].

As mentioned above, there are several forms of ionizing radiation: alpha, beta and neutrons as particulate forms, and gammas and x-rays as electromagnetic forms. Alpha particles (i.e., the nuclei of helium) are emitted when decays occur in energetically unstable heavy nuclei. The alpha decay process is shown in Equation (1), where X and Y represent the initial and final elements along with the emitted alpha particle [3, p. 6].

$$ {}^{A}_{Z}X = {}^{A-4}_{Z-2}Y + {}^{4}_{2}\alpha \tag{1} $$

Beta decays result in the emission of fast electron or beta particles. The decay process is shown in Equation (2) where X and Y again represent the initial and final elements along with the emitted beta particle and $\bar{\nu}$ is the antineutrino [3, p. 3]. Beta decays can also include the emission of a positron rather than an electron.

$$ {}^{A}_{Z}X \rightarrow {}^{A}_{Z+1}Y + \beta^{-} + \bar{\nu} \tag{2} $$

The antineutrino has a very low probability of interacting with matter, although it carries energy away from the reaction. The recoil nucleus Y has a relatively small recoil energy, generally below the ionization threshold. Thus, the most practical way to detect a beta decay is by detecting the fast electron itself.

X-rays are emitted when orbital electrons change energy states. When an electron is excited, it enters a higher energy orbital. However, electrons in an atom have a tendency to return to their natural ground state. When an electron returns to its lower energy ground state an X-ray photon is emitted [3, p. 15].

Excited nuclei emit gamma rays “in their transition to lower-lying nuclear levels” [3, p. 11]. This often follows beta decays. Four examples of common gamma reference sources are shown in Figure 1.

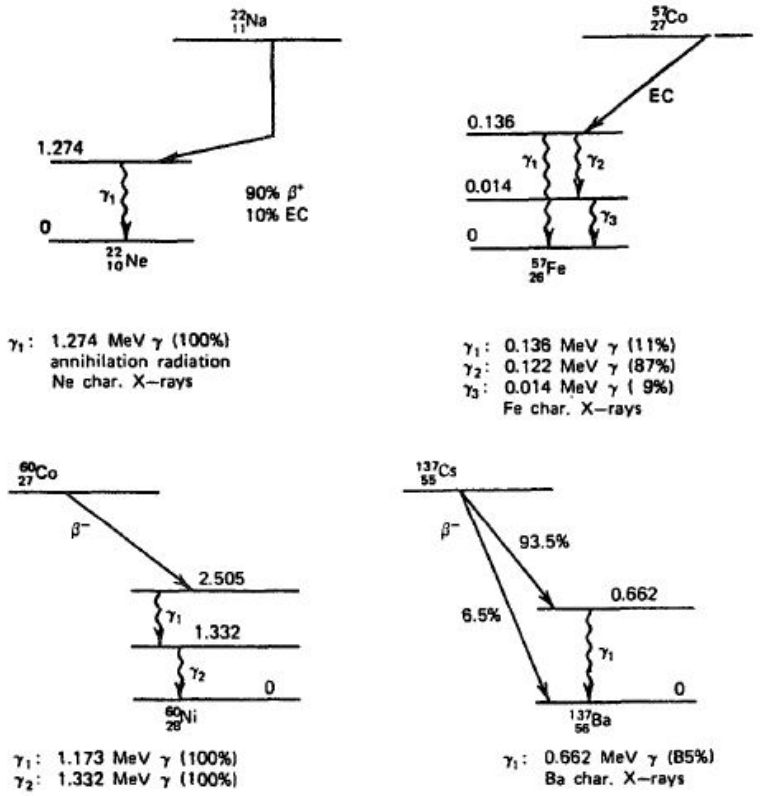

Figure 1. Decay schemes for some common gamma reference sources.
Source: [3, p. 11].

Each of these examples shows a beta decay which results in a new excited nucleus. This excited nucleus emits a gamma ray to return to a stable state. Gamma rays are also often emitted after nuclear reactions as seen in Equation (3).

$$ {}^{4}_{2}\alpha + {}^{9}_{4}Be \rightarrow {}^{12}_{6}C^{*} + {}^{1}_{0}n \tag{3} $$

In this example, after the collision of the alpha particle with the beryllium nucleus, the resulting carbon nucleus is left in an excited state. The carbon nucleus emits a gamma ray to return to a stable state. Another possible reaction is:

$$ {}^{4}_{2}\alpha + {}^{13}_{6}C \rightarrow {}^{16}_{8}O^{*} + {}^{1}_{0}n\,. \tag{4} $$

In this reaction, the oxygen is left in an excited state and subsequently emits a gamma ray [3, p. 13].

These events laid the groundwork for modern radiation detection. This thesis focuses specifically on the use of a polymer that is sensitive to ionizing radiation employed as a capacitor dielectric. This radiation-sensitive dielectric material is incorporated in a micro-electromechanical system (MEMS) package to enable a low cost yet versatile detection system. The framework used by Korostynska et al.[4] has been followed during this thesis.

A. APPLICATIONS OF RADIATION DETECTORS

Radiation detectors can be used in a wide variety of applications to include medicine [5], [6], the nuclear power industry [3], mining and geologic characterization, environmental studies, and homeland security [7].

The earliest form of radiation usage in medical imaging was x-rays. Modern medical imaging can be broken into three categories. The first is based on “transmission measurements using an external beam source” [5]. The transmission beam penetrates the material at a certain depth according to its density and atomic number. As a result, the transmitted beam shows the material composition. A second method involves the introduction of a radiation source into the body. This radioactive pharmaceutical is directed towards certain areas of the body. The radioactive material is absorbed by certain tissues of interest, and in addition to damaging the targeted tissue, the emitted radiation can also be measured. A third medical application involves “measurements not using [ionizing] radiation” [5]. While ionizing radiation is very useful in many forms of medical imaging, it can cause serious unintended damage to specific organs or the whole body. Therefore,

using non-ionizing radiation imaging techniques (such as Magnetic Resonance Imaging, MRI) pose less risk to internal organs or to the human body as a whole [5].

The nuclear power industry requires the use of radiation detection to fulfill a diverse set of requirements. For example, “industrial research at the University of Glasglow’s Nuclear Physics Group primarily focuses on assessment of legacy waste containers using cosmic muon tomography and development of miniature detector systems for the characterization of nuclear facilities during the decommissioning process” [3].

Radiation detection is important to determine exposure levels in environments where humans live. Ionizing radiation exposure can result from both natural and artificial sources. Some examples of natural environmental radiation applications include radon detection, or the establishment of “exposure limits for workers or pilots and checking radiation levels in food…” [5]. An important method of radiation detection is the use of thermoluminescent dosimeters (TLD). Service members often use these dosimeters as a form of passive radiation detection. When radiation reacts with a TLD, the ionization process modifies the structure of the detection medium and enables electrons to exist in an energized state. The TLD can be heated to cause the electrons to return to their ground state and emit light. This light is measured by a photomultiplier and is proportional to the accumulated radiation exposure [6].

Radiation detection plays a vital role in homeland security. Radiation detection serves as a tool for finding illicit materials entering the country. For example, radiation detection is used to screen “shipments at their point of origin and on their arrival at a United States port” [7]. X-rays are used to find radioactive materials in well-shielded items that need further inspection. For detecting fissionable materials, several techniques are available, generally by inducing fission in the target material using neutrons or high-energy photons. One such technique “involves an intense beam of 14 MeV neutrons from a D-T generator” [7]. Another method uses a pulsed photonuclear neutron detector. This detector uses energized photons that cause fission in the material releasing detectable neutrons, fission products and associated gamma radiation.

In particular, gamma ray detection is important to this thesis. This form of detection is important to personal dosimetry, area dosimetry, and characterization of a radiation environment. Illicit nuclear materials often emit gamma rays as well. While neutron interactions are not a specific focus of this thesis, neutrons often interact with nuclei resulting in the emission of gamma rays. Some examples of places sensitive gamma sensors can be used are harbors and customs areas to screen incoming and outgoing material.

B. THESIS STRUCTURE AND EXPERIMENT OUTLINE

The four chapters of this thesis outline the procedure taken to further our understanding of gamma-sensitive polymers and their interaction with ionizing radiation. Chapter I has introduced this thesis by providing a brief background on the history of radiation detection and its applications. Chapter II provides a background on key areas including micro-electrical mechanical systems (MEMS), radiation physics, and capacitor physics. Chapter III outlines the experimental methods and results. It discusses specific procedures and results for several iterations of experiments. Chapter IV discusses conclusions and provides insight on future work for this thesis.

THIS PAGE INTENTIONALLY LEFT BLANK

II. BACKGROUND

This chapter provides technical background information relevant to the research by addressing three topic areas. First, it discusses micro-electrical mechanical systems (MEMS) application and advantages. Second, it discusses radiation basics. Specifically, it will focus on gamma interaction with material. Third, it discusses capacitor physics and the theory behind dielectric materials.

A. MICRO-ELECTRICAL MECHANICAL SYSTEMS (MEMS)

Micro-electromechanical systems (MEMS) combine mechanical and electrical components into small-integrated devices. These devices are important because they have the ability to generate signals detectable on the macro scale based on micro scale phenomena. MEMS incorporates four key components: microstructures, microsensors, microactuators, and microelectronics. Microsensors are responsible for detecting "changes in the system's environment by measuring mechanical, thermal, magnetic, chemical or electromagnetic information or phenomena" [8, p. 2]. This information is then sent to the microelectronics to be processed. The microelectronics then "signal the microactuators to react and create some form of changes to the environment" [8, p. 2].

MEMS offers several advantages as compared to traditional manufacturing techniques. First, MEMS has extended to a range of devices and connected previously unrelated fields. Second, the fabrication technique has increased the reliability and performance of components and devices. Third, it simply produces components that cannot be made by any other method [8, p. 3]. Fourth, MEMS sensors can be integrated with and built during the same process as microelectronics. An example of this is the lab-on-a-chip device that integrates laboratory functions on a chip as seen in Figure 2.

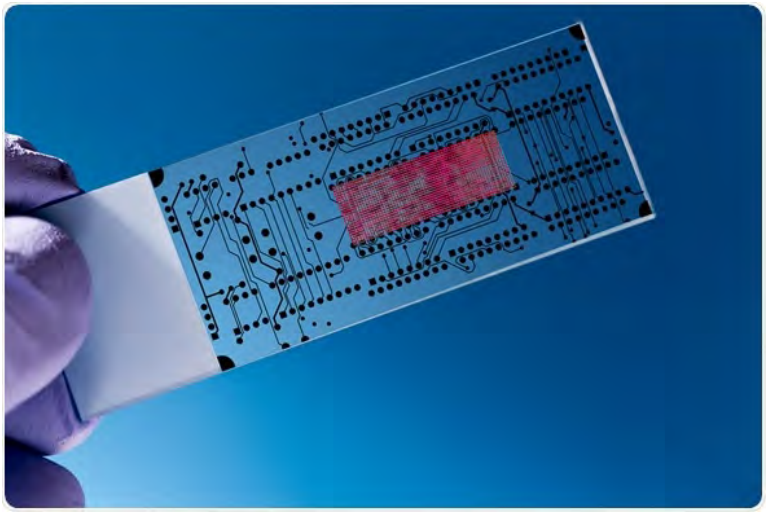

Figure 2. Lab-on-a-chip device. Source: [9].

MEMS devices can be either sensors or actuators. A sensor is defined as "a device that measures information from a surrounding environment and proves an electrical output signal in response to the parameter it measured" [8, p. 4]. Sensors are involved in six different energy domains: mechanical, thermal, chemical, radiant, magnetic, and electrical. Actuators are defined as devices that convert "an electrical signal into an action" [8, p. 4]. A sensor or actuator can also be called a transducer. A transducer is defined as "a device that transforms one form of signal or energy into another form" [8, p. 4]. For example, it can transform a detected gamma photon energy into an electrical signal to be sent to another system for interpretation.

B. RADIATION BASICS

Radiation is defined as "energy given off by matter in the form of rays or high-speed particles" [10]. There are two types of radiation: electromagnetic and particle radiation. Electromagnetic radiation consists of pulsating waves of electrical and magnetic energy [10]. Some examples of this form of radiation are x-rays, radar, radio waves, and visible light. Particle radiation involves "tiny fast-moving particles that have both energy and mass (weight)" [10]. Some examples of this form of radiation are alpha particles, beta particles, and neutrons [10].

Each form of radiation differs in its ability to penetrate materials. Important factors include the energy of the particle or photon and the corresponding electric charge. For example, alpha particles have relatively low penetration due to their electric charge, while electromagnetic photons and neutral particles (e.g., gamma photons and neutrons) are more penetrating due to their lack of electric charge. In general, the higher the energy of the photon or particle, the greater its penetration as seen in Figure 3 [3, p. 1].

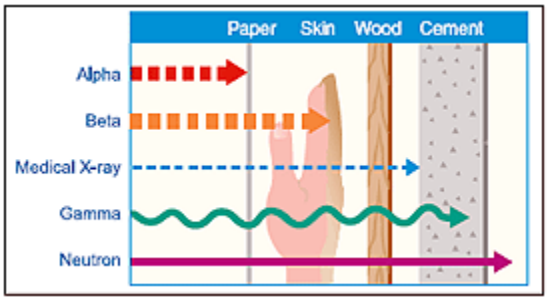

Figure 3. Radiation penetration. Source: [10].

For this thesis, the primary concern is gamma radiation. Gamma rays interact with matter in three ways: photoelectric absorption, Compton scattering, and pair production.

In photoelectric absorption, the incoming photon interacts with the absorbing atom. The photon is absorbed by one of the electrons in an atom. The electron absorbing a gamma photon can acquire enough energy to break free from its atom and an energetic photoelectron is ejected from the absorber atom as seen in Figure 4 [3, pp. 48–49].

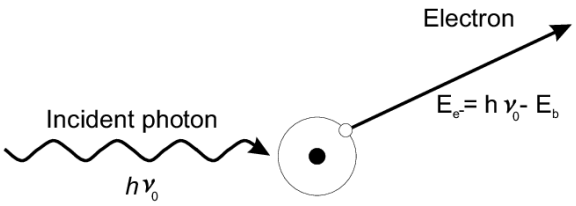

Figure 4. Photoelectric absorption. Source: [11].

The energy of the energetic photoelectron can be represented with Equation (5).

$$E_{e-} = h\nu - E_b \tag{5}$$

$E_b =$ binding energy of the photoelectron in its original shell

$h =$ Planck's constant = 6.626e-34 Js

$\nu =$ frequency of photon (Hz)

Compton scattering occurs when the incident gamma ray collides with the electron transferring some of its energy as seen in Figure 5. The electron, now known as a recoil electron, deflects at an angle from the direction of the incoming photon (angle in Figure 5) whereas the gamma ray deflects at a different angle (angle shown in Figure 5). Compton scattering is a common mechanism for radioisotope sources [3, pp. 50–51].

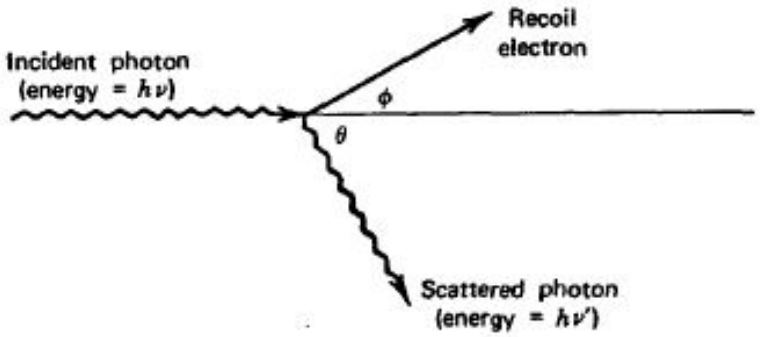

Figure 5. Compton scattering. Source: [3, p. 51].

The energy of the scattered photon can be calculated using Equation (6).

$$h\nu' = \frac{h\nu}{1 + \frac{h\nu}{m_0 c^2 (1 - \cos\theta)}} \tag{6}$$

$m_0 c^2$ = rest-mass energy of the electron (0.511 MeV)

Pair production occurs when an electron-positron pair replaces the gamma-ray photon. Subsequently, the electron-positron pair undergoes annihilation. This interaction is energetically possible when "the gamma-ray energy exceeds twice the rest-mass energy of an electron (1.02 MeV)" [3, p. 51]. The three types of interactions described above occur at different energy levels as shown in Figure 6.

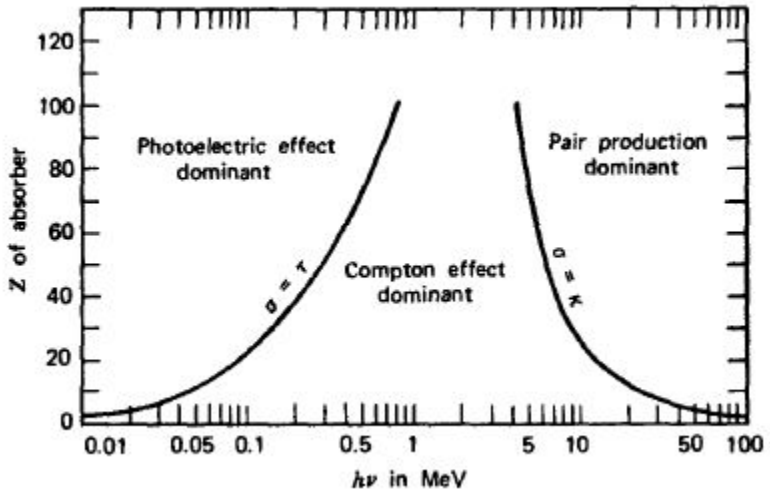

The lines show the values of Z and hv for which the two neighboring effects are just equal

Figure 6. The relative importance of the three major types of gamma-ray interaction. Source: [3, p. 52].

Dose is often used to describe how much radiation a material absorbs. When exposed to the same gamma rays, different materials will absorb different amounts of energy depending on the physical properties of the material. The absorbed dose is defined as "the energy absorbed from any type of radiation per unit mass of the absorber" [3, p. 59]. The historic unit is defined as a rad (100 ergs/gram). Currently, the most commonly used unit, the SI unit, is the gray (Gy) or one joule/kilogram. These two units are shown in Equation (7).

$$1 \text{ Gy} = 100 \text{ rad} \tag{7}$$

C. CAPACITORS AND DIELECTRIC MATERIALS FOR GAMMA SENSING

1. Capacitors

Capacitors are systems that store electrical charge. They generally consist of two conductors separated by a non-conductive medium. The capacitance of a system can be calculated using the Equation (8).

$$C = \frac{Q}{V} \tag{8}$$

C = capacitance (Farad)

Q = charge (Coulomb)

V = potential (V)

A simple form of a capacitor is a parallel plate. This kind of capacitor consists of two parallel plates of conductive material, separated by a dielectric. Gauss's law can be used in Equation (9) to calculate the parallel plate capacitance [12, p. 51].

$$V = -\int E \cdot dl \tag{9}$$

Using Gauss's law, the parallel plate capacitance can be represented using Equation (10) [12].

$$C = \varepsilon \frac{\varepsilon_0 A}{d} \tag{10}$$

ε = relative permittivity or dielectric constant of the material between the two capacitor plates

ε_0 = permittivity of free space = $8.85 \times 10^{-12}\ {}^{F}\!/_{m}$

A = area of capacitor (m^2)

d = distance between plates (m)

If, in a given capacitor system, the area and distance between the capacitor plates are kept constant, the capacitance can still be changed because of changes occurring within the dielectric material between the plates. In our case, material changes from the absorption of ionizing radiation in the dielectric will result in a measurable change in the capacitance of the capacitor.

2. Dielectric Background and Interaction

The dielectric in a capacitor serves as a way to decrease "the electric field produced by a given charge density" [13].

$$E_{effective} = E - E_{polarization} = \frac{\sigma}{\varepsilon \times \varepsilon_0} \tag{11}$$

σ = charge per unit area

ε_0 = permittivity of free space = $8.85 \times 10^{-12}\ {}^{F}\!/_{m}$

ε = relative permittivity or dielectric constant

As seen in Figure 7, a material generally contains polar molecules oriented in random directions. The presence of an electric field reorients the polar molecules to polarize the material. The dielectric should be a good electric insulator to prevent any current leakage in the capacitor as seen in Figure 7.

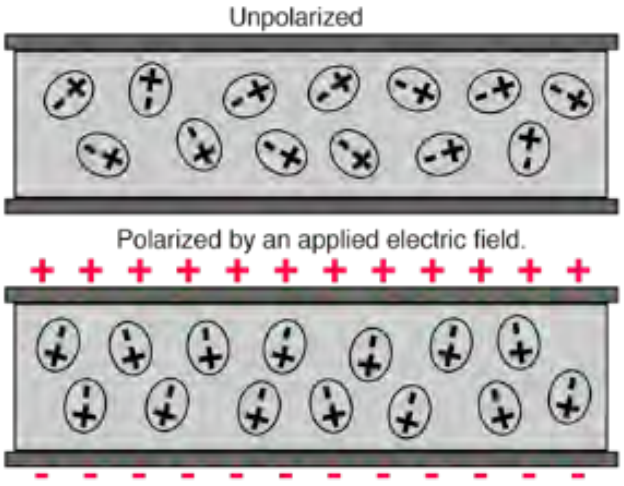

Figure 7. Dipole orientation in a dielectric material in the presence of an electric field. Source: [13].

A dielectric of particular interest for detection of gamma radiation is polyvinylidene difluoride (PVDF). PVDF can be described as "a semicrystalline polymer that shows excellent mechanical and chemical properties and thermal and electrical stabilities" [14]. It is created by polymerizing 1,1-difluoroethylene ($CH_2=CF_2$) as seen in Figure 8.

Figure 8. Polymerization of PVDF. Source: [15].

There are five possible crystal combinations of PVDF: α, β, γ, δ, and ε. Different crystallization conditions such as “mechanical deformation, poling under large electric fields, annealing or crystallization at high temperatures” [14] yields different crystal forms. The most common crystal forms for PVDF are α and β. In crystal form α, “the chains are packed in the unit cell in such a way that the molecular dipoles are anti-parallel and there is no net (crystal) dipole” [14]. In crystal form β, “the chains are packed in the unit cell in such a way that the dipoles associated with individual molecules are parallel, leading to a non-zero dipole moment of the crystal” [14]. The α and β phase can be seen in Figure 9.

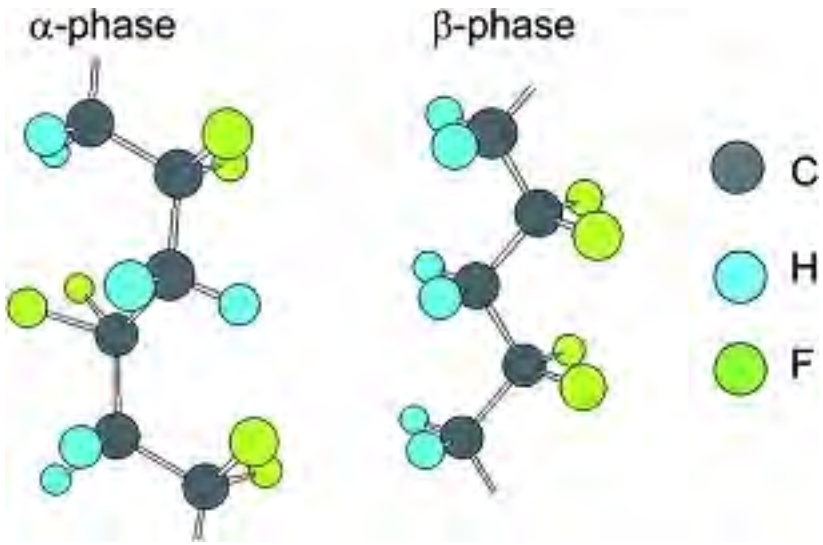

Figure 9. Alpha- and beta-phase structure of PVDF. Source: [15].

THIS PAGE INTENTIONALLY LEFT BLANK

III. EXPERIMENTAL METHODS AND RESULTS

The future goal of the research described in this thesis is to produce a MEMS capacitor device as seen in Figure 10. This MEMS capacitor chip operates with a set of interdigitated fingers. The fingers are used to create a large surface area and increase the overall capacitance. The distance is kept as a constant between the fingers. By applying the dielectric paste in between the fingers, one can measure the change in capacitance after exposure to ionizing radiation.

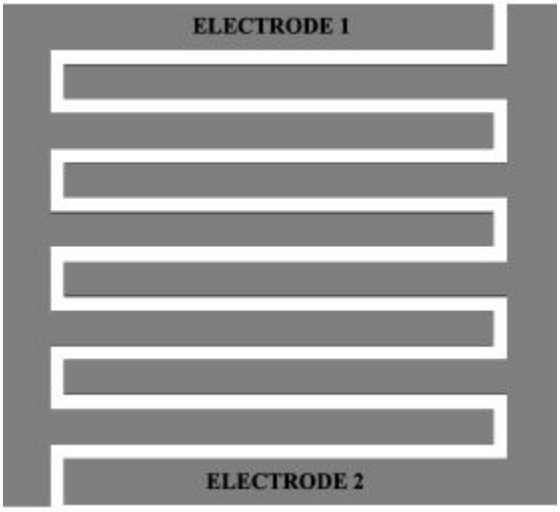

Figure 10. Design of an interdigitated finger sensor. Source: [16, p. 26].

Hameed and Gats successfully created the MEMS capacitor chip as shown in Figure 11. While Hameed and Gats successfully manufactured the MEMS capacitor chip, the dielectric material used was not sensitive enough to ionizing radiation. The experiments in this thesis focused on finding a dielectric material that exhibits enhanced sensitivity to ionizing gamma radiation.

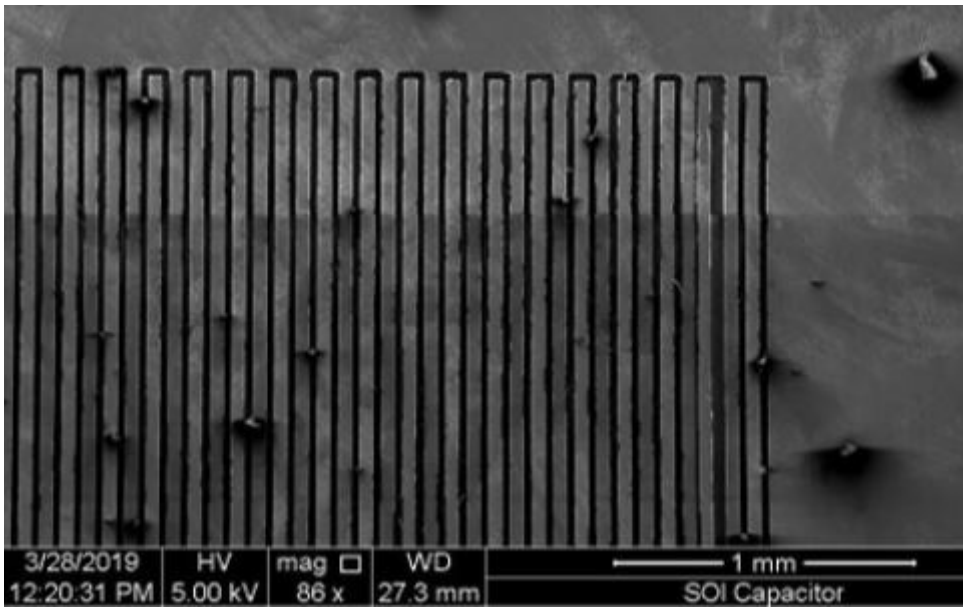

Figure 11. Top-down SEM image of capacitor chip. Source: [16, p. 30].

This chapter describes the methodology behind the several iterations of testing conducted in this thesis research. Each sub section focuses on test sensor fabrication, data analysis, and sensor modifications. The three iterations of testing were those using copper plates, acrylic plates, and aluminum plates. Aluminum plates proved to be the most successful. As a result, four different iterations were done using the aluminum plates. During each iteration, lessons were learned and modifications were made on subsequent iterations. The progression of this chapter reflects the actual progression of the experiments conducted in this thesis research.

A. CALCULATIONS

There are several calculations that are important to this experiment. First, it is important to calculate the dose to be applied the test device to enable direct comparison to previous results published in scientific articles. It is standard for scientific articles to use the dose rather than the elapsed time to present data. Second, the data in these experiments is normalized to demonstrate how the new capacitance resulting from the radiation exposure compared to the capacitance of the unirradiated control device.

1. Dose

To calculate the dose in this experiment, the initial radioactivity of the Cs-137 (0.25 μCi) source was used. This value was converted to Becquerels using Equation (12).

$$1\mu Ci = 37000 Bq \tag{12}$$

A Becquerel is defined as one decay per second. After this conversion, the Equation (13) was used to calculate absorbed dose rate in units of Watts/kg.

$$ADR = R_{Cs-137} \times E_{\gamma} \times 1.60218 \times 10^{-13} \frac{J}{MeV} \times \frac{\Omega}{4\pi} \tag{13}$$

ADR = absorbed dose rate (W/kg)

R_{Cs-137} = initial radioactivity of Cs-137 (Bq)

E_γ = gamma peak energy (MeV)

Ω = solid angle (sr)

The gamma peak energy for Cs-137 is 0.662 MeV as determined by the RSS8-EU 8 Disk Source Set. The solid angle is measured from a point to the surface of a sphere as seen in Figure 12. For this thesis, the Cs-137 source was treated as a point source and it was assumed that it irradiated half of a sphere. This gives the solid angle 2π since the distance between the capacitor and the source is almost zero. Furthermore, the area of the capacitor is quite larger than the coin source.

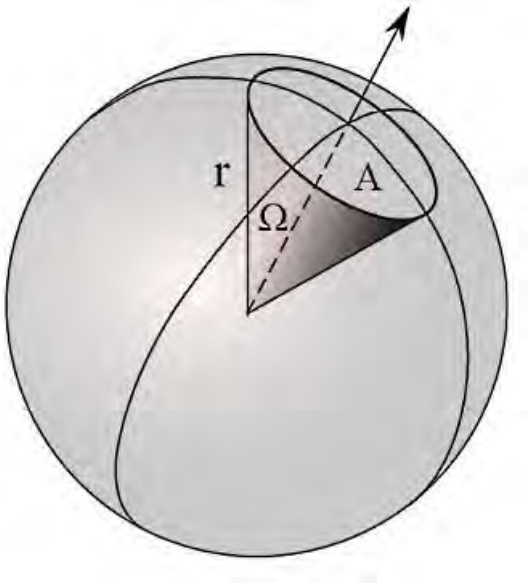

Figure 12. Solid angle representation. Source: [17].

By knowing the amount of time elapsed, the dose can be calculated in Grays (J/kg) using Equation (14).

$$AD = ADR \times t \tag{14}$$

AD = absorbed dose (J/kg)

ADR = absorbed dose rate (W/kg)

t = time (sec)

2. Normalized Values

The normalized values were used to compare the new capacitance to the original capacitance. Normalized values are used to account for potential differences between the control and exposed capacitances stemming from the differences in the process of mixing and preparation. The normalized value is calculated using Equation (15).

$$\text{Normalized Capacitance} = \frac{C_m}{C_i} \tag{15}$$

C_m = measured capacitance

C_i = initial capacitance

It also allowed for the comparison between the capacitor exposed to the radiation source and the control capacitor. The difference was calculated using Equation (16).

$$Difference = C_{Cs-137} - C_{control} \tag{16}$$

C_{Cs-137} = capacitance of Cs-137 exposed sample

$C_{control}$ = capacitance of control

B. DIELECTRIC PASTE

In order to make the dielectric paste, a modified procedure created by Korostynska et al. was used [4]. The following materials were used in preparing the dielectric: carbon black, surfactant, ethyl cellulose, N-Methyl-2-Pyrrolidone (NMP), and polyvinylidene difluoride (PVDF). VULCAN® XC72R Specialty Carbon Black was used to improve the dielectric constant and the sensitivity to gamma radiation. It was found that pure PVDF paste was an insulator [4]. The surfactant homogenously dispersed the carbon black. NMP served as the solvent for the paste. PVDF was the polymer that reacted with the gamma radiation.

In the first iteration on creating the paste, 6 wt. % carbon black, 7 wt. % ethyl cellulose, and 1 wt. % surfactant was used. The initial proportions for the copper plates can be seen in Table 1.

Table 1. Initial proportions for copper plates

Material	Weight (g)
VULCAN® XC72R Specialty Carbon Black	0.12
Ethyl Cellulose	0.14
Surfactant	0.02
PVDF	1.72
Add NMP to dissolve	

After 24 hours of allowing the paste to dry, it was found that the solidified paste lacked the structural integrity to hold the two copper plates together. The paste at this point was too dry and crumbled as seen in the Figure 13.

Figure 13. Copper plate capacitor disassembly

It was concluded that too much carbon black had been used, and in the next iteration, the weight percentage of the carbon black would be reduced to overcome this issue.

In the second iteration, the carbon black was reduced to 3 wt. % and the rest of the material weight percentages were kept the same. This mixture enabled the copper plates to adhere to each other after allowing the paste to dry. The final proportions can be seen in Table 2.

Table 2. Final proportions for copper plates

Material	Weight (g)
VULCAN® XC72R Specialty Carbon Black	0.3
Ethyl Cellulose	0.7
Surfactant	0.1
PVDF	8.9
Add NMP to dissolve	

C. COPPER PLATE

1. Procedure

The first method used to create a capacitor was based on using copper plates as the conductor. One larger and one smaller circular copper plate (approximately one inch and a half-inch diameter, respectively) were created. The PVDF dielectric paste was created and applied between the two copper plates. An even force was applied to the plates to ensure an equal distribution of dielectric paste across the face of the plate. Excess paste was left outside the smaller plate to ensure there was no contact between the large and small copper plates as seen in Figure 14.

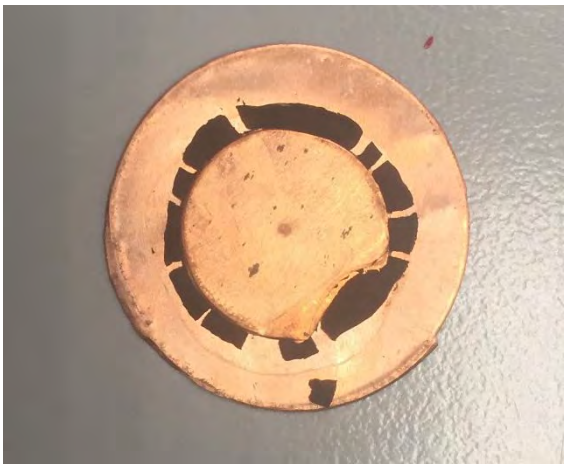

Figure 14. Copper plate capacitor

Wires were soldered to the smaller and larger copper plate to allow for easy measurements. A binder clip was used to bind the copper plates to a Cesium-137 point source as seen in Figure 15.

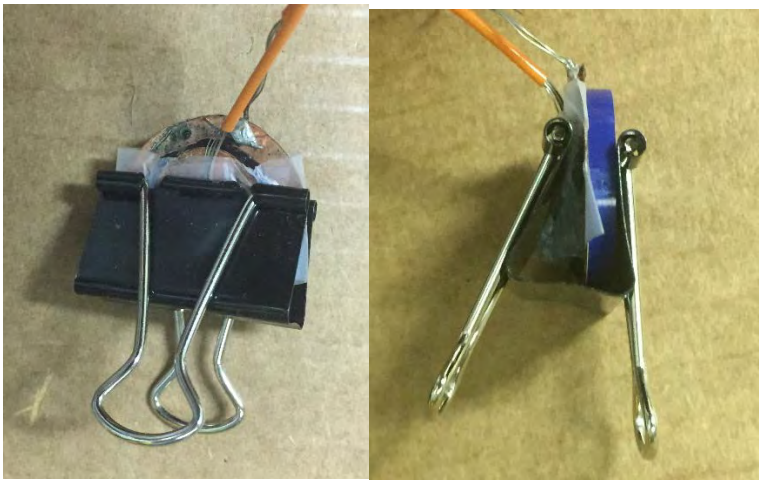

Figure 15. Bound copper plates

The bound copper plate was placed inside the lead shielding as seen in Figure 16.

Figure 16. Lead shielding for copper plate

The capacitance was measured approximately every 24 hours and recorded. The devices used to measure the capacitance were ELENCO LCR-1810 and BK PRECISION 875A as seen in Figure 17 and Figure 18, respectively.

Figure 17. ELENCO LCR-1810

Figure 18. BK PRECISION 875A

2. Results and Discussion

An experiment was conducted with the copper plate capacitor based on a 3 wt % carbon doped paste and a Cs-137 source. The results can be seen in Figure 19 and Figure 20. The initial results indicated that there was an exponential decrease in the capacitance over time. The capacitance appeared to flat line after about 300 hours at 0.10 nF. This was about a 93% decrease from the initial capacitance of 1.415 nF. This decrease warranted further investigation into the effect of the Cs-137 source on the dielectric paste. We believe the natural degradation of the paste was responsible for the decrease in the capacitance. There was no control to compare the results to in this iteration to see the effects of the Cs-137 source. It was determined that a control would need to be added to future experiment iterations.

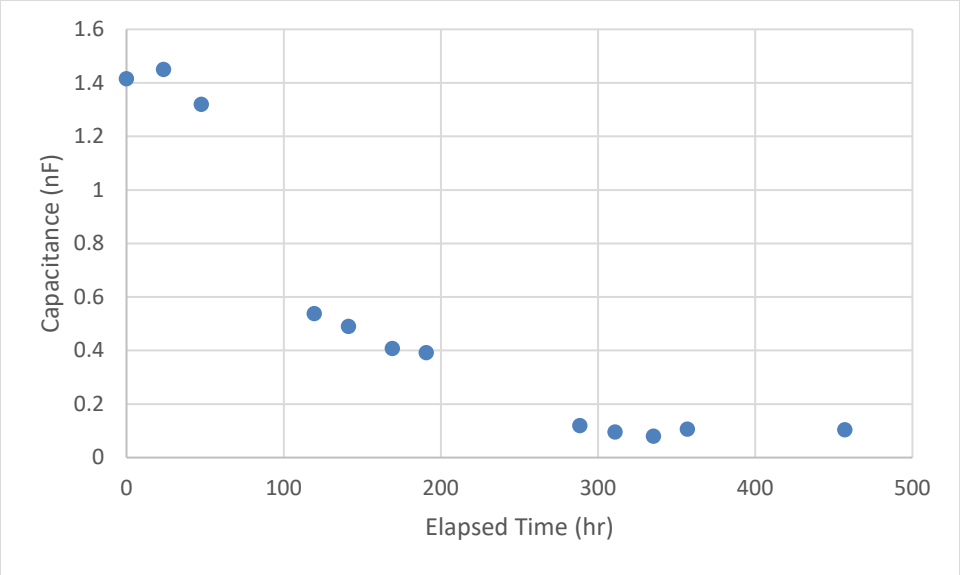

Figure 19. Copper plate Cs-137 capacitance (nF) vs. elapsed time (hr)

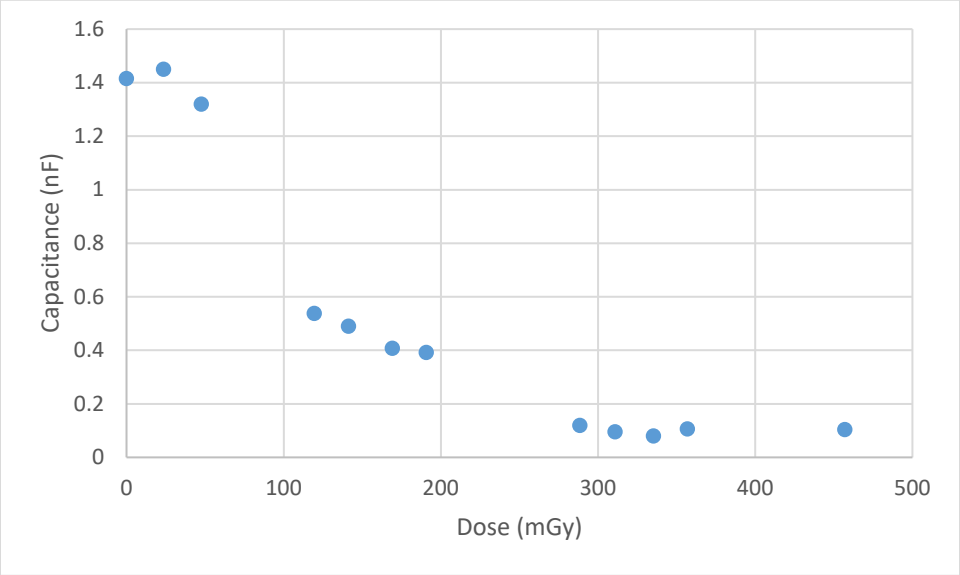

Figure 20. Copper plate Cs-137 elapsed time (hr) vs. dose (mGy)

D. ACRYLIC PLATE

1. Procedure

Acrylic plates were used in an attempt to bind the copper plates together. Two acrylic plates and screws were used as seen in Figure 21.

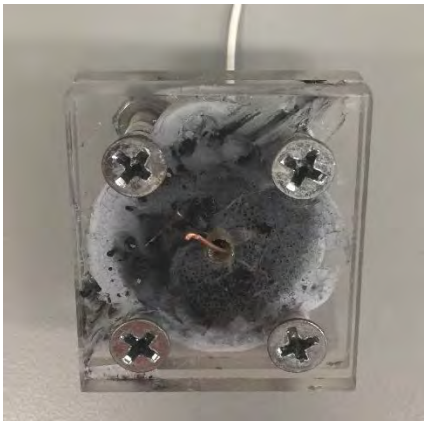

Figure 21. Acrylic plate assembly

2. Results and Discussion

This method proved to be the most difficult for several reasons. First, it was difficult to apply an even force with the screws to ensure an even distribution of the dielectric paste. Second, the copper plates kept slipping when the screws were being tightened. Third, wires were needed to provide a connection to the copper plates under the acrylic plates. The wires were difficult to place under the acrylic plates. Fourth, this assembly did not ensure electrical separation between the copper plates. This was discovered when low resistance was measured between the copper plates indicating the plates were touching. Because of these difficulties, this method was abandoned, and irradiation measurements were not performed.

E. ALUMINUM FOIL

1. Procedure

Due to the failure of the acrylic plates and the need to expand on the original study with the copper plates, another approach was taken using aluminum foil and paper with an added control. The procedure on the Instructable Circuits website [18] was modified to create the capacitor. First, aluminum was cut using the following dimensions as seen in Figure 22. The thickness of the aluminum foil was 0.016 mm.

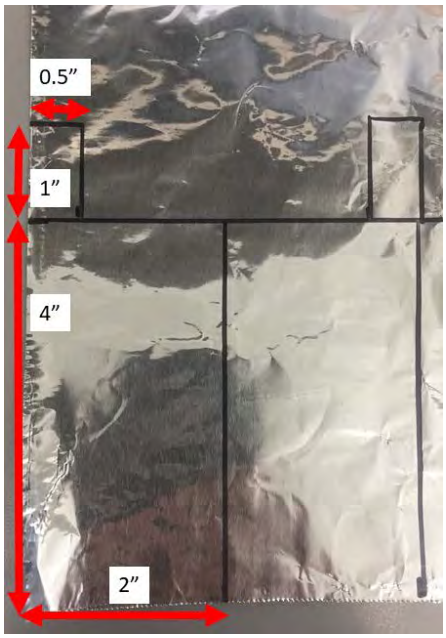

Figure 22. Aluminum foil dimensions

The cut aluminum foil can be seen in Figure 23. After the aluminum foil was cut, the paper was marked with the dimensions in the Figure 24.

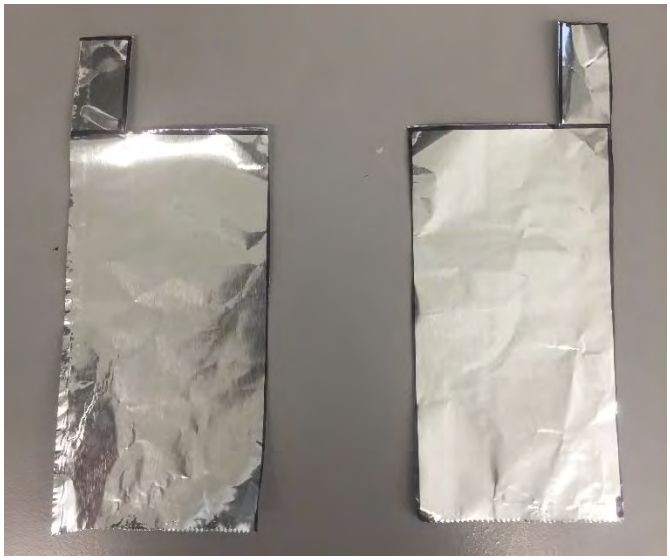

Figure 23. Cut aluminum foil

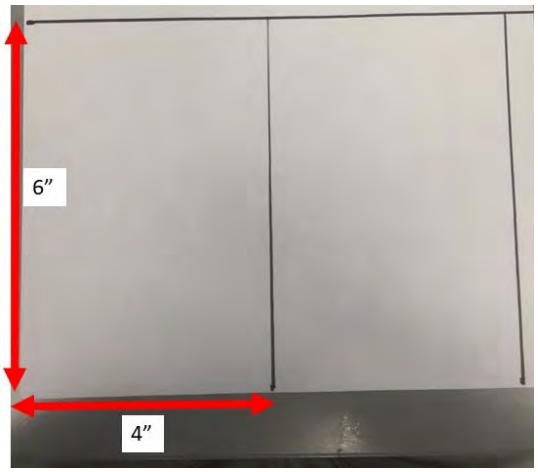

Figure 24. Paper dimensions

For the first iteration, a standard size sheet of paper was used between the two aluminum pieces. One piece of aluminum foil was taped to one side of the paper so the small aluminum flap extended past the edge of the paper. This aluminum flap was used as the connection for the multimeter. A small amount of paper was left between the larger area of the aluminum foil and the edge to ensure there was not a short circuit between the two pieces of aluminum foil. An example set up can be seen in the Figure 25.

Figure 25. Aluminum foil on paper

On the opposite side of the paper to the aluminum foil, the dielectric paste was evenly spread on the area where the aluminum was taped. The second piece of aluminum foil was taped over the dielectric paste mirroring the piece of aluminum foil on the other side. The electrical contact flaps were placed on opposite sides to ensure there would not be a short circuit. Finally, the cut pieces of paper were taped over the aluminum foil to insulate the capacitor. The completed set up can be seen in the Figure 26 and Figure 27.

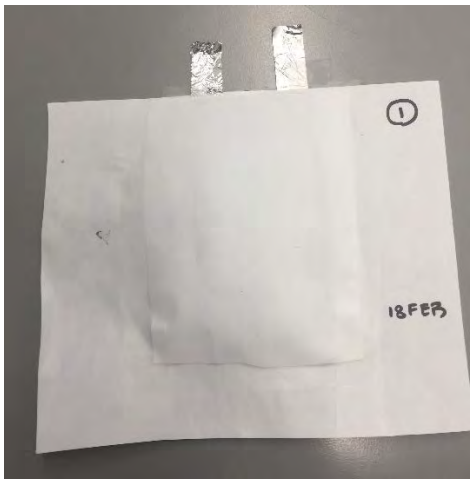

Figure 26. Aluminum foil capacitor #1

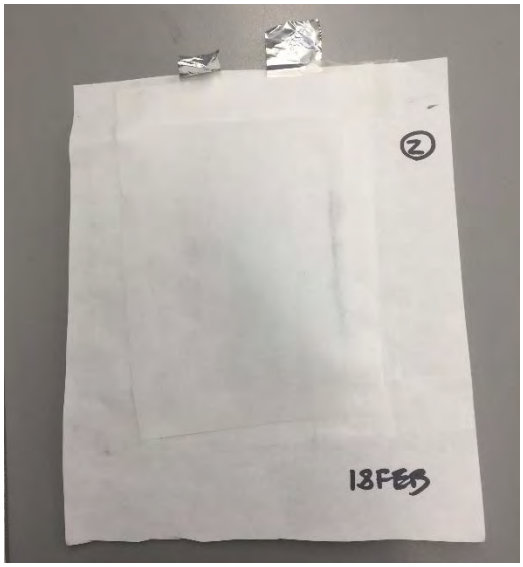

Figure 27. Aluminum foil capacitor #2

It was determined that using the paper as a medium did not provide proper insulation. The resistance measured between the two pieces of aluminum foil indicated a short circuit. It was hypothesized that the paper had been saturated by the paste and ripped. This exposed the pieces of aluminum foil to each other. The next iteration of this model used plastic as the insulating medium.

The same procedure outlined above was followed for cutting the plastic material and aluminum foil. Standard size Ziploc sandwich bags (6.5” x 5.875”) were used as the plastic medium. The Ziploc part of the bag was cut off as seen in the Figure 28.

Figure 28. Cut sandwich bag

After the sandwich bag was cut, one piece of aluminum foil was taped to one side of the plastic as seen in Figure 29.

Figure 29. Aluminum foil taped to capacitor

On the other side without the foil, the dielectric paste was evenly applied along the area of the aluminum foil. The second piece of aluminum foil was taped over the dielectric paste. Afterwards, paper was taped over the aluminum foil to provide a protection as seen in Figure 30.

Figure 30. Paper on top of aluminum

Cardboard and binder clips were used to clamp the sample as shown in Figure 31.

Figure 31. Completed plastic capacitor

Two capacitors were assembled with one being exposed to the Cs-137 source and the other being an unirradiated control. The capacitor exposed to the Cs-137 source was placed under a lead shield as seen in Figure 32. The control capacitor was placed in a drawer remote from the radiation source. The capacitance was measured approximately every 24 hours.

Figure 32. Cs-137 capacitor under lead shield

2. Iteration 1

The experiment was conducted using a 3 wt % carbon doped dielectric paste. Figure 33 shows the change in capacitance over time for the Cs-137 irradiated capacitor and the unirradiated control. Figure 34 shows the same information as a function of the received dose. Each capacitor showed an initial spike in capacitance. This was likely a result of the dielectric paste being compressed by the cardboard and binder clips. The distance between the capacitor plates initially decreased, thus, increasing the overall capacitance. However, once the dielectric paste reached an equilibrium, both capacitors exhibited a decrease in capacitance over time. This was likely a result of the polymer degrading. Exposure to the atmosphere causes the dielectric paste to dry out. It is important to note that the rate at

which the capacitance changed was different though. The radiation-exposed capacitor exhibited a slower decay as compared to the control.

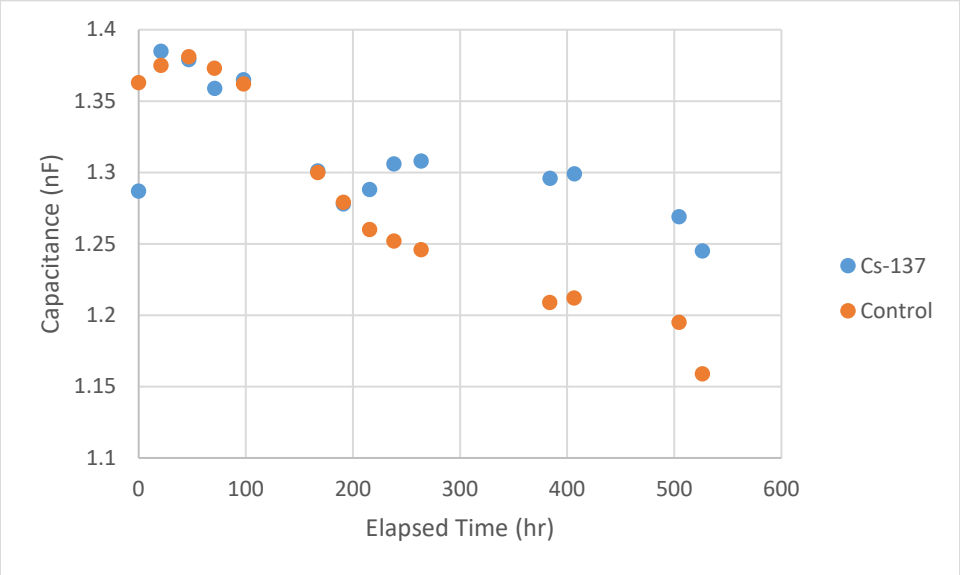

Figure 33. Iteration 1: Capacitance (nF) vs. elapsed time (hr)

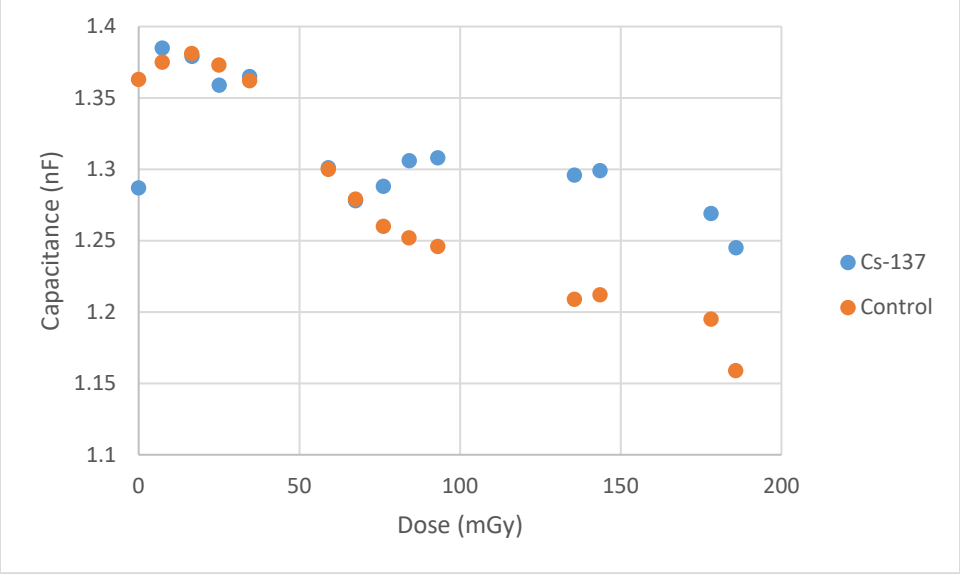

Figure 34. Iteration 1: Capacitance (nF) vs. dose (mGy)

Figure 35 shows the capacitance percent change as a function the elapsed time. The capacitance percent was based on the initial capacitance measurement for each respective capacitor. For the first 100 hours, each capacitor showed an increase in capacitance. The Cs-137 capacitor showed a greater percent increase. After 100 hours, the control capacitor showed a percent decrease in capacitance while the Cs-137 capacitor remained relatively neutral. This indicated that there was indeed a difference between the two capacitors. The effect of Cs-137 gamma exposure was counteracting the degrading nature of the dielectric paste to keep a consistent capacitance.

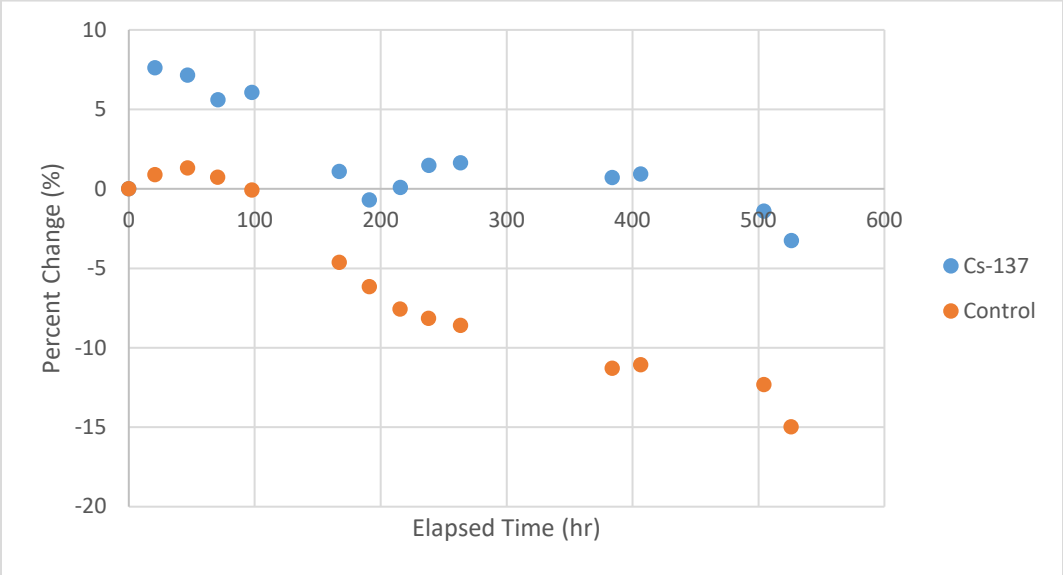

Figure 35. Iteration 1: Capacitance percent change (%) vs. elapsed time (hr)

Figure 36 shows the normalized values for each capacitor. Figure 37 and Figure 38 show the difference in these normalized values. As discussed previously, the normalized values were a ratio between the measured capacitance and the initial capacitance. The difference in normalized values reinforces that there was a significant difference in the capacitances of the two capacitors.

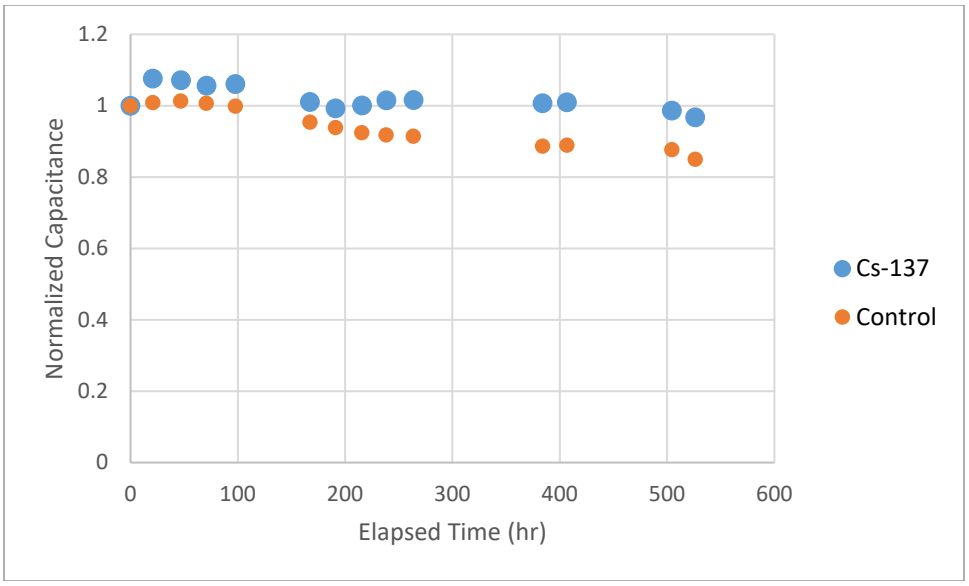

Figure 36. Iteration 1: Normalized capacitance vs. elapsed time (hr)

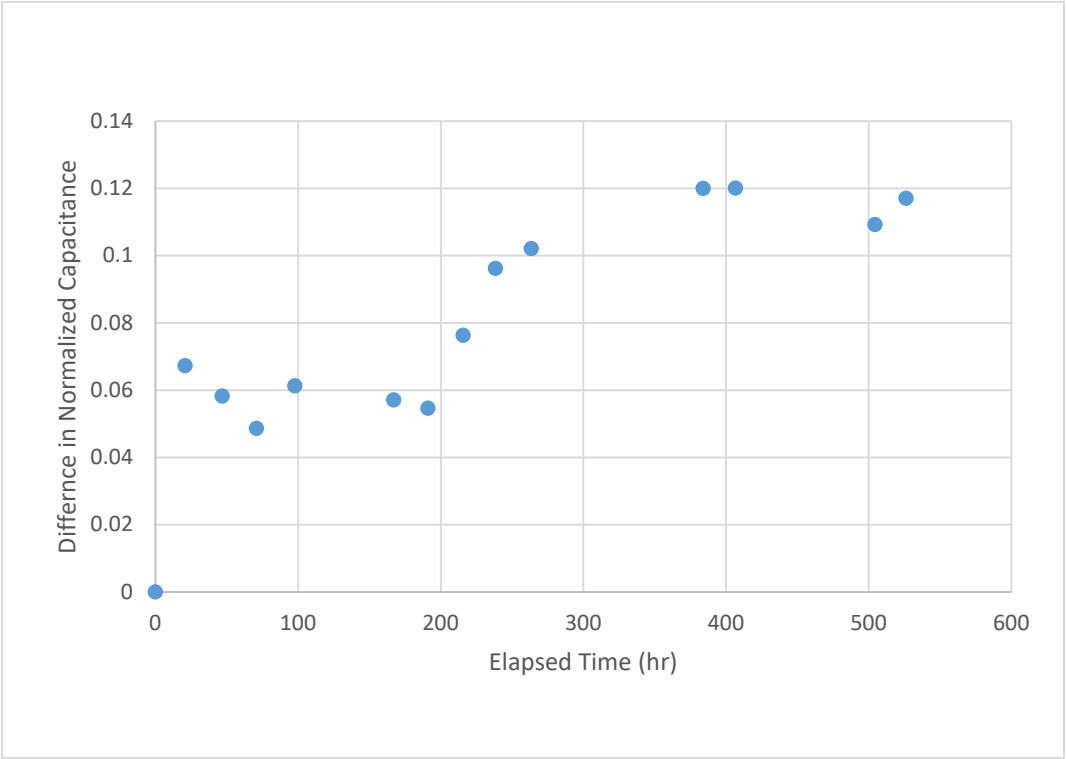

Figure 37. Iteration 1: Difference in normalized capacitance vs. elapsed time (hr)

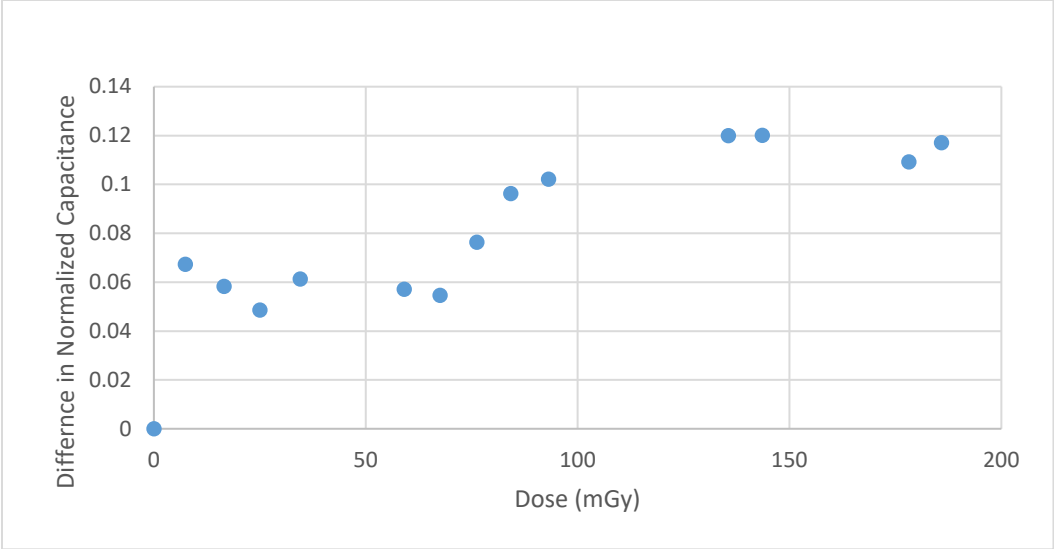

Dose only applies to the irradiated sample

Figure 38. Iteration 1: Difference in normalized capacitance vs. dose (mGy)

Figure 39 shows the reference plot for the PVDF sample in the Korostynska et al. paper [4]. It was expected that the capacitance of the PVDF sample would increase after about 3 mGy of radiation. However, iteration one did not follow this trend and instead showed an overall decrease in capacitance over an extended duration.

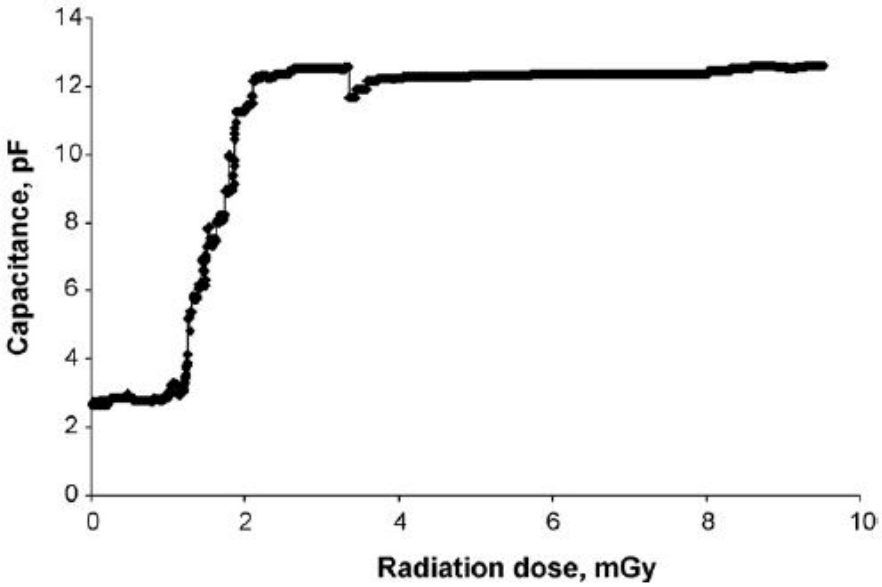

Figure 39. Reference plot for PVDF sample. Source: [4].

3. Iteration 2

A second iteration was conducted in order to determine the replicability of the experiment. In order to account for any differences coming from the lead weight being placed on top of capacitors, both capacitors were placed under lead shields as shown in Figure 40. Additionally, more measurements were taken at the beginning of the experiment to determine if there were any short-term effects.

Figure 40. Iteration 2: Setup of capacitors

Figure 41 shows the capacitance as a function of time and dose respectively. Initially, both capacitors started at difference values. The Cs-137-exposed capacitor started at 1.324 nF whereas the control capacitor started at 1.162 nF. These differences are likely a result of each capacitor having a different amount of dielectric paste. Normalizing the values to initial values was done to account for the difference between the two. Additionally, each capacitor exhibited an increase in capacitance for the first few hours. This did not indicate any short-term effects of the radiation source on the dielectric paste. The control capacitor continued to increase in capacitance whereas the capacitor that was to be exposed to Cs-137 leveled off at around 1.333 nF.

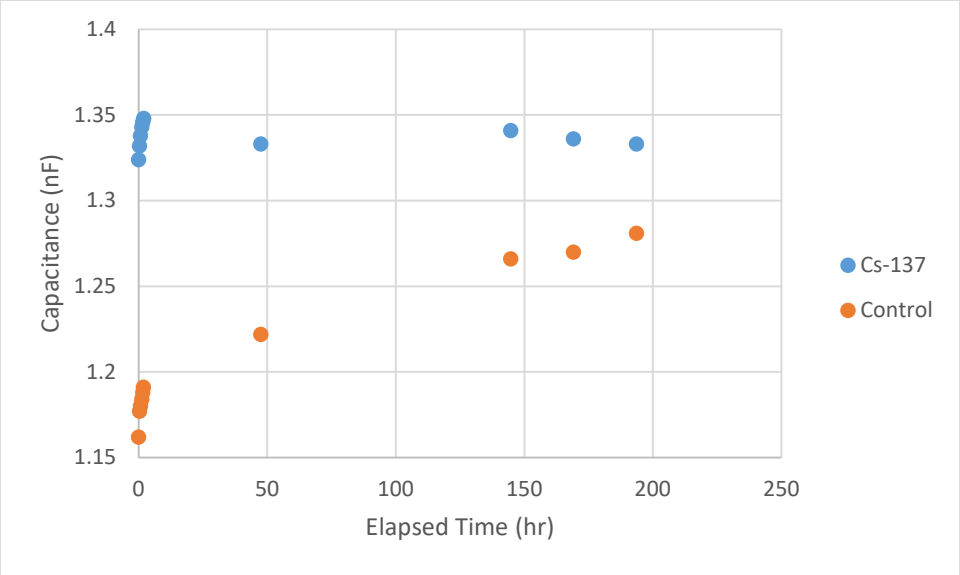

Figure 41. Iteration 2: Capacitance (nF) vs. elapsed time (hr)

As seen in Figure 42, after the beginning of exposure of one of the capacitors to Cs-137, each capacitor displayed an increase in capacitance. However, the control device displayed a larger percent increase in capacitance as compared to the Cs-137-exposed device. This differed from the results in iteration one. In iteration one, the Cs-137 exposed device displayed a larger percent increase in capacitance. This difference may be a result a different experimental set up. During iteration one, the control capacitor was placed in a drawer whereas, the Cs-137-exposed capacitor was placed under a lead shield. In iteration two, both capacitors were placed under the lead shield. While the lead shield protected the capacitors from background radiation, it also served as a weight compressing the dielectric paste and increasing the capacitance. The following iteration ensured both capacitors are set up under the lead shield to create uniformity in the experiment.

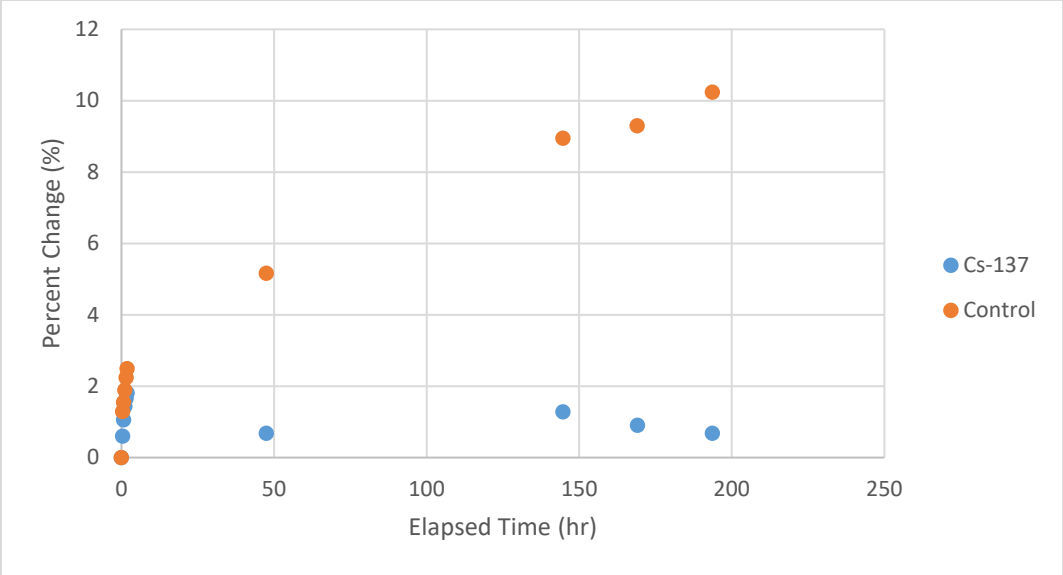

Figure 42. Iteration 2: Capacitance percent change (%) vs. elapsed time (hr)

Figure 43 shows the normalized values as a function of the elapsed time. These figures reaffirmed the previous conclusion that the control capacitor experienced a greater increase in capacitance as compared to the Cs-137-exposed capacitor.

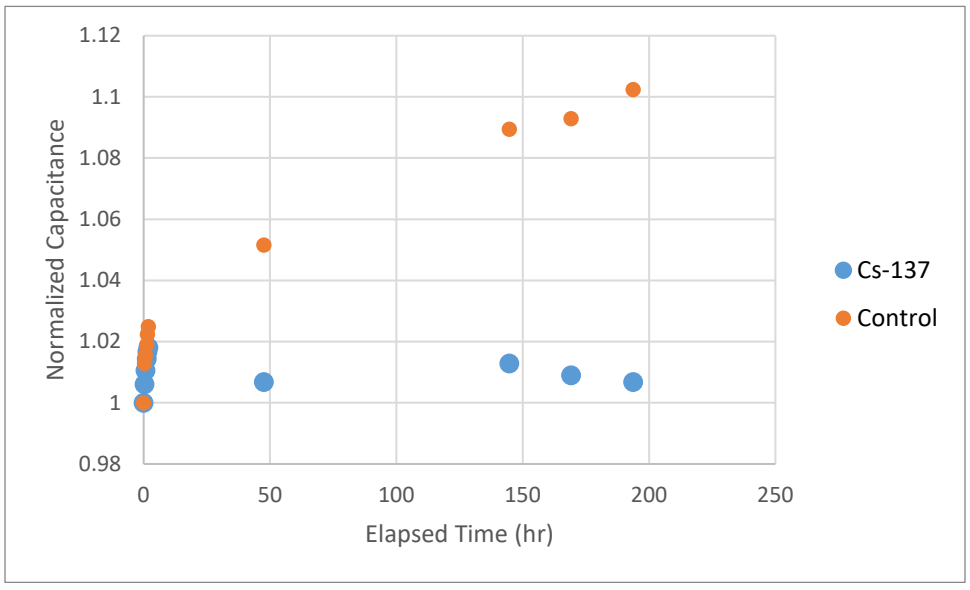

Figure 43. Iteration 2: Normalized capacitance vs. elapsed time (hr)

Figure 44 and Figure 45 show the difference in normalized values between the control capacitor and Cs-137-exposed capacitor. It can be concluded that there was a difference between the normalized values. This indicated a significant difference in capacitances.

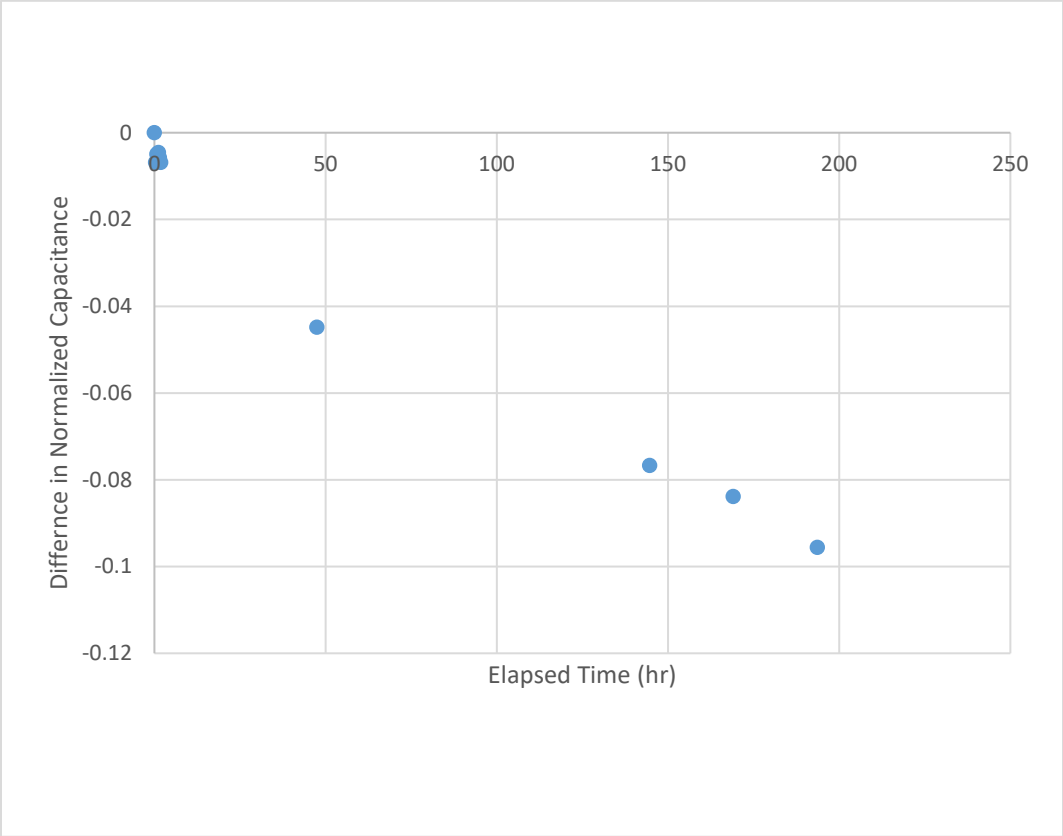

Figure 44. Iteration 2: Difference in normalized capacitance vs. elapsed time (hr)

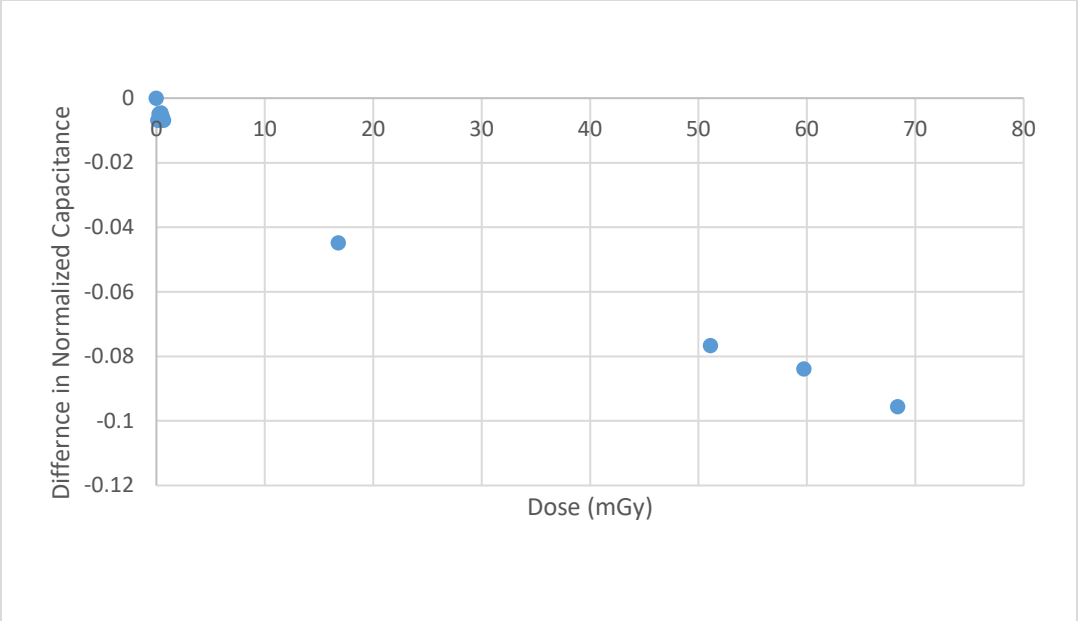

Dose only applies to the irradiated sample

Figure 45. Iteration 2: Difference in normalized capacitance vs. dose (mGy)

4. Iteration 3

A third iteration was conducted by using the two previous control capacitors. Both capacitors were placed under lead shields as done in iteration two and allowed to compress over three days. This period ensured changes in capacitances were not a result of the dielectric being compressed and the distance between the capacitor plates changing. Additionally, the Cs-137 source was placed outside the cardboard rather than inside as seen in Figure 46.

Figure 46. Cs-137 source placed outside cardboard

A quarter was placed on top of the cardboard to determine if the weight of the Cs-137 source would alter the capacitance. It was determined that the weight of the Cs-137 source was not a factor in the capacitance change.

Figure 47 shows the capacitance as a function of the elapsed time and dose respectively. Despite the control starting at a higher capacitance, its capacitance decreased over time. On the other hand, the Cs-137-exposed capacitor displayed an increase in capacitance over time.

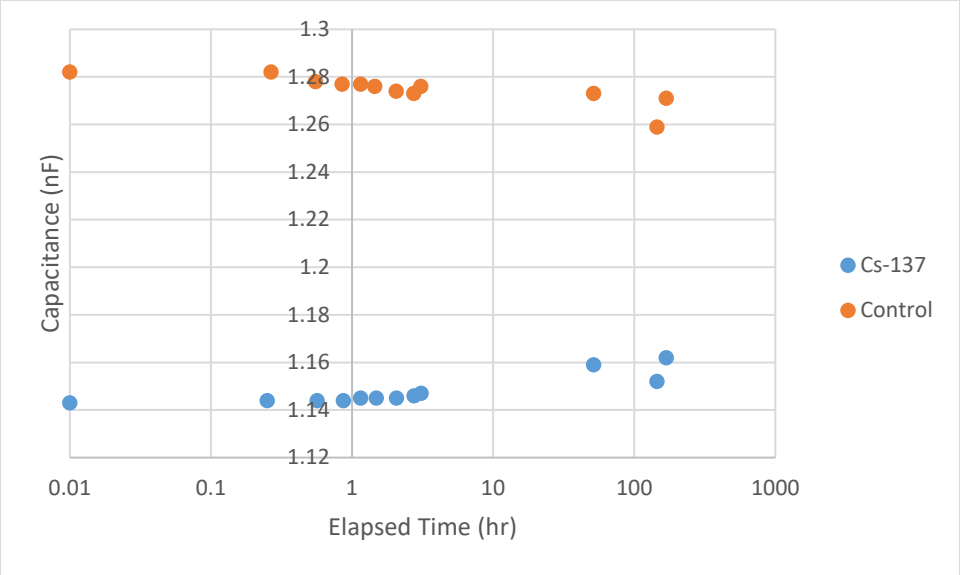

Figure 47. Iteration 3: Capacitance (nF) vs. elapsed time (hr)

Figure 48 shows the capacitance percent change as a function of the elapsed time and dose respectively. The Cs-137-exposed device displayed a net increase in capacitance whereas the control displayed a net decrease in capacitance.

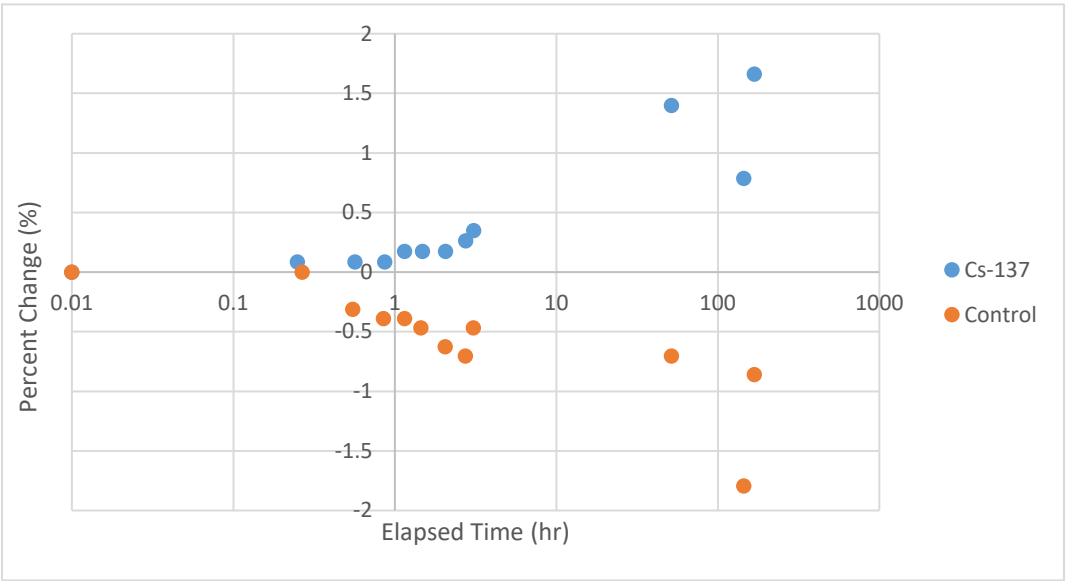

Figure 48. Iteration 3: Capacitance percent change (%) vs. elapsed time (hr)

Figure 49 shows the normalized values as a function of the elapsed time. It reaffirmed the previous conclusion that the Cs-137 capacitor experienced a greater increase in capacitance as compared to the control capacitor.

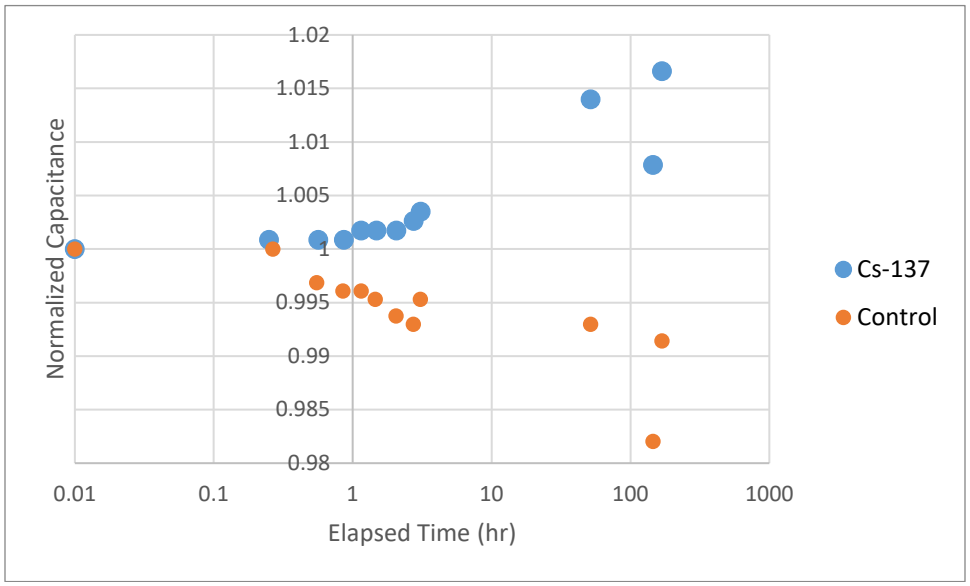

Figure 49. Iteration 3: Normalized capacitance vs. elapsed time (hr)

Figure 50 and Figure 51 show the difference in normalized values. It can be concluded that there is a significant difference in the normalized values of the capacitors.

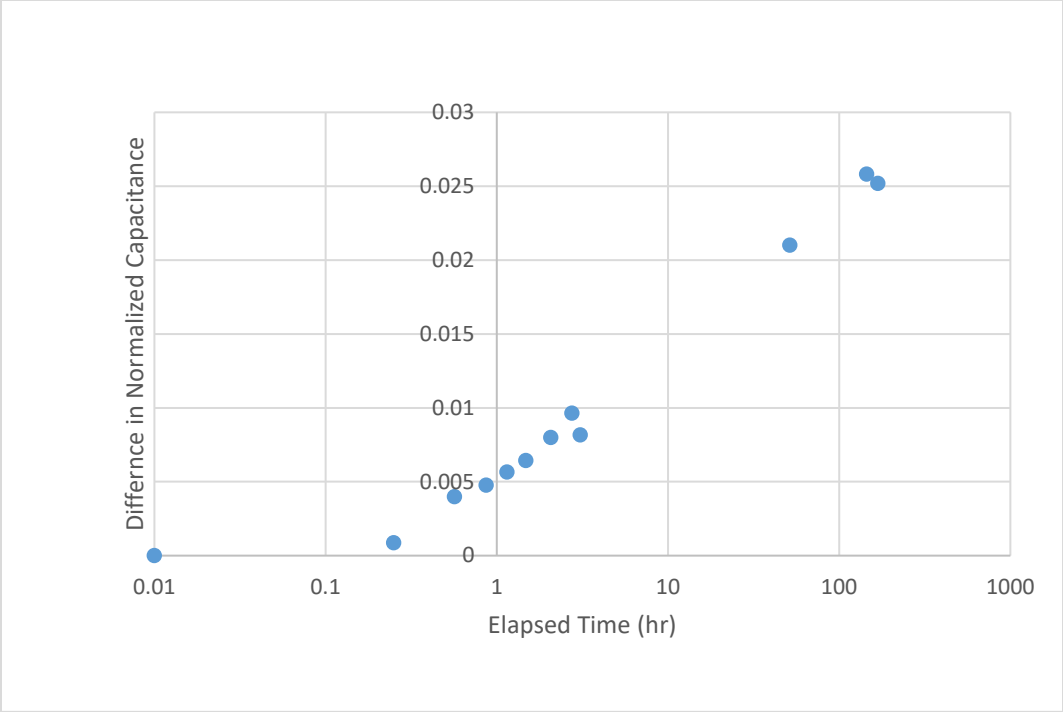

Figure 50. Iteration 3: Difference in normalized capacitance vs. elapsed time (hr)

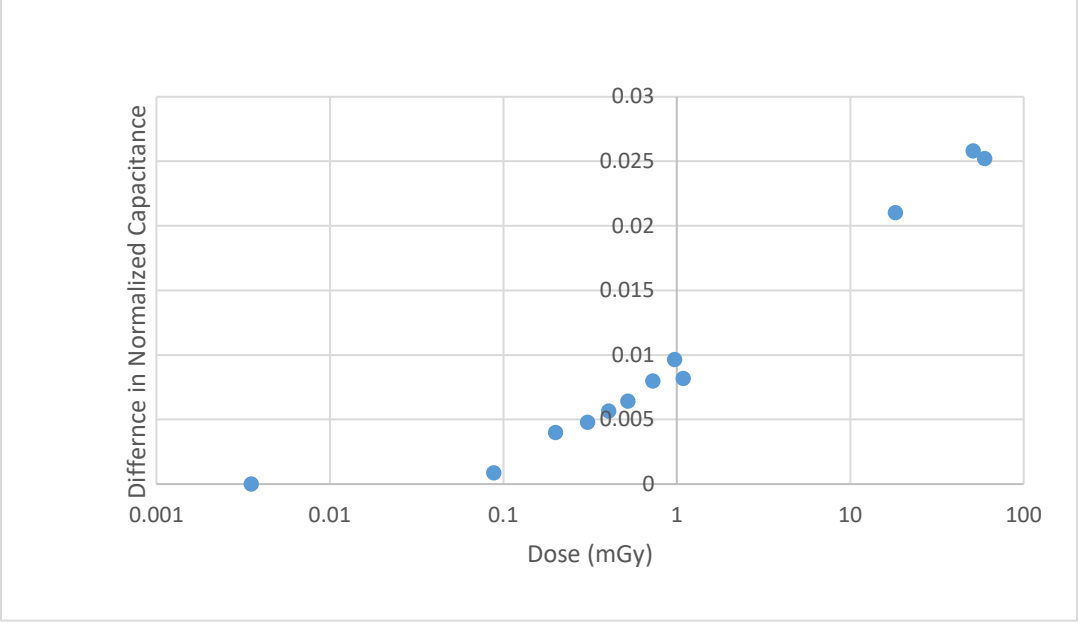

Dose only applies to irradiated sample

Figure 51. Iteration 3: Difference in normalized capacitance vs. dose (mGy)

These results closely aligned with the results in Iteration 1. This is promising because modifications were made to limit external factors that could influence the observed changes. Both capacitors were placed in the same environment and under the same lead shield. The only difference between the capacitors were the exposure to a Cs-137 source. It is important to note that the capacitance for both capacitors followed the same trend of decrease and increase over a long term as seen in Figure 47 and Figure 48. This indicates that that there may be a dependence of capacitance on a common environmental factor, like the temperature and or humidity. This could affect the dielectric constant of the paste. In subsequent iterations of this experiment, temperature and humidity were recorded to see how they might affect the capacitance. Additionally, an experiment were conducted comparing two control capacitors to verify consistency between the capacitances.

5. Iteration 4

Iteration 4 was conducted using 3 wt % carbon doped dielectric paste. The procedure for iteration 3 was followed with the following additions. First, the temperature and humidity were recorded in this experiment. The point of these measurements was to determine if humidity and temperature changed the capacitance of the device. Second, an experiment was conducted comparing two control capacitors to determine similarity in capacitances when not exposed to a Cs-137 source.

The results for comparison between the two controls are seen in Figure 52, Figure 53, Figure 54, and Figure 55.

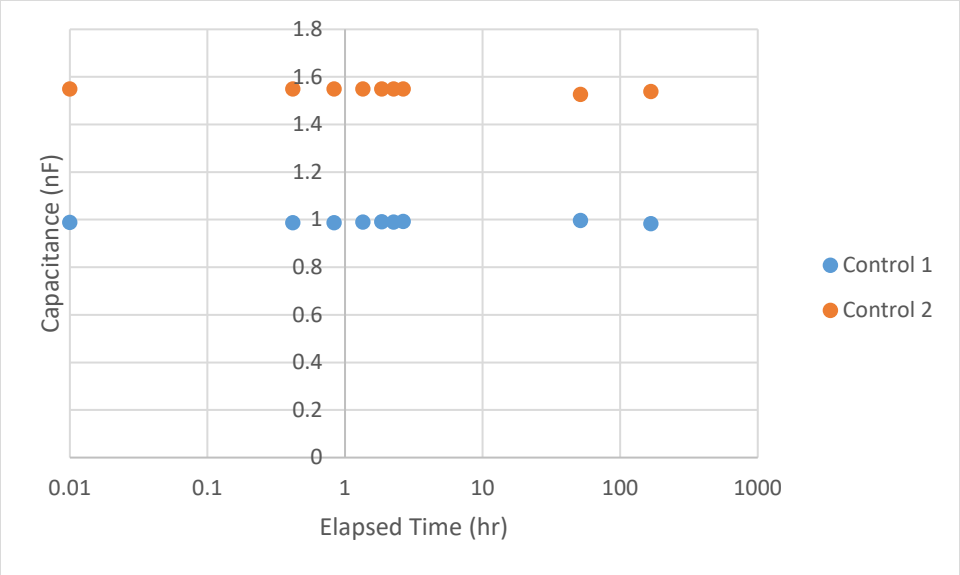

Figure 52. Iteration 4: Control comparison capacitance (nF) vs. elapsed time (hr)

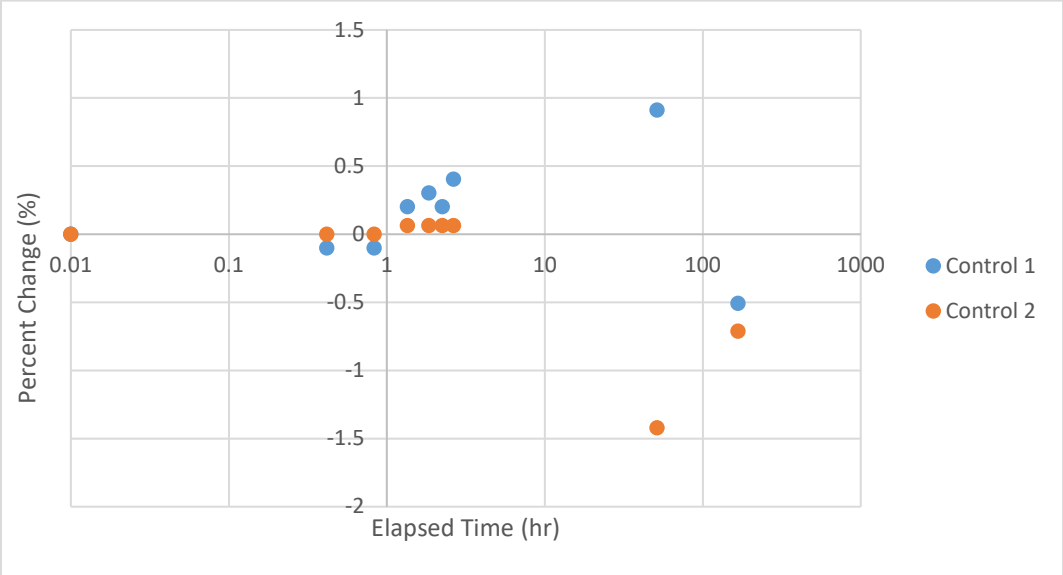

Figure 53. Iteration 4: Control comparison capacitance percent change (%) vs. elapsed time (hr)

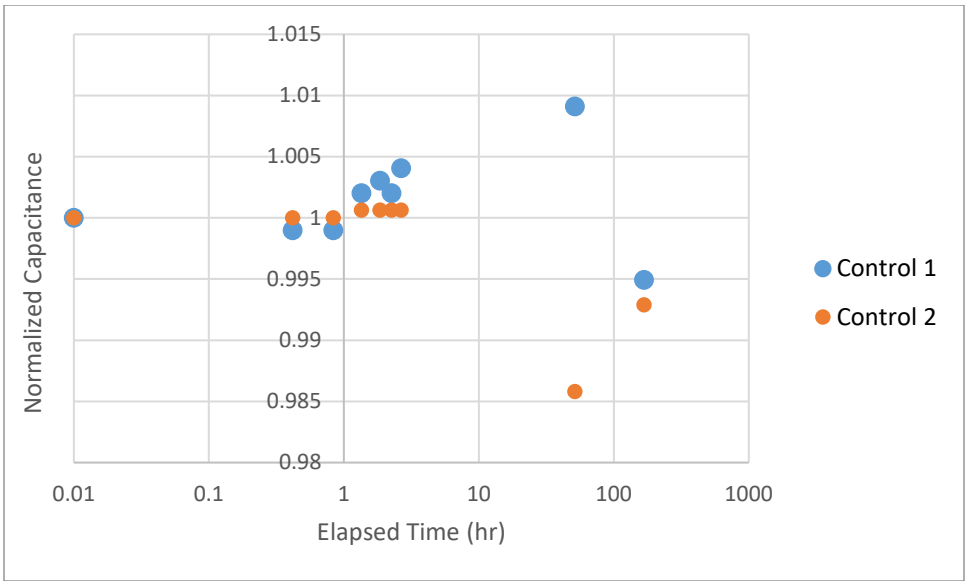

Figure 54. Iteration 4: Control comparison normalized capacitance vs. elapsed time (hr)

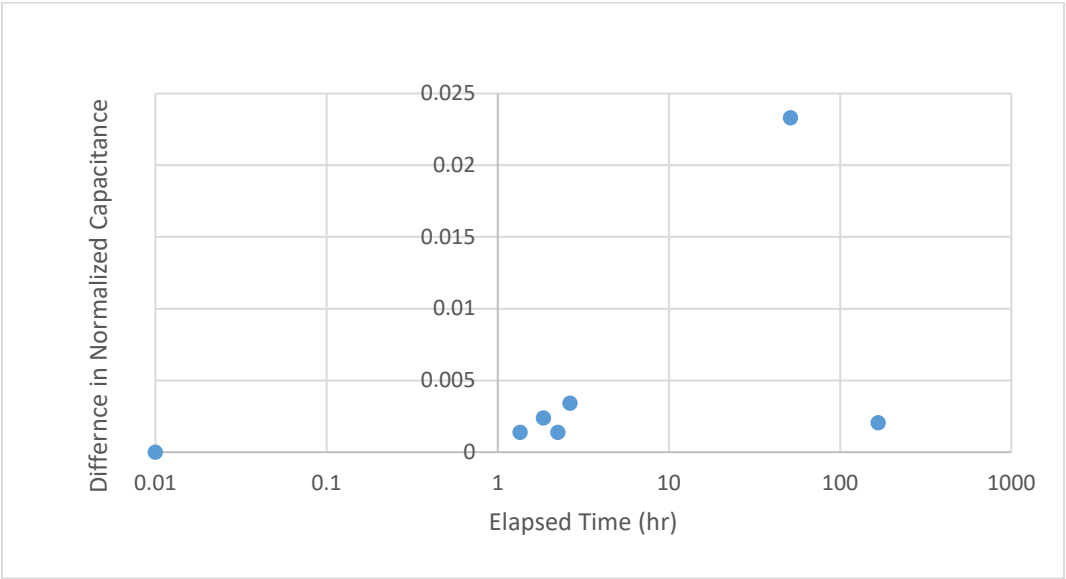

Figure 55. Iteration 4: Control comparison difference in normalized capacitance

The results indicated that there was no significant change in capacitances between the two controls. Additionally, the temperature and humidity remained relatively constant throughout the experiment. If the same conditions are held when the capacitor is exposed to the Cs-137 source, any changes in capacitance should be a result of the gamma radiation exposure.

After the control comparison, the Cs-137 source was added. Figure 56 shows the capacitance as a function of time and dose respectively. Each capacitor started at largely different capacitances. This was likely a result of a different amount of dielectric in each capacitor.

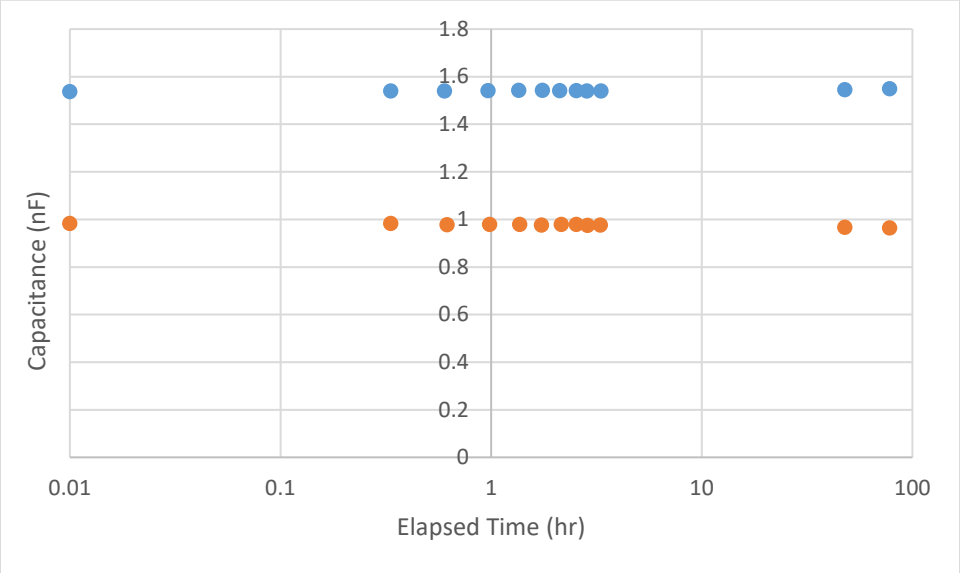

After the introduction of Cs-137

Figure 56. Iteration 4: Capacitance (nF) vs. elapsed time (hr)

Figure 57 shows the capacitance percent change as a function of time and dose respectively. There is a clear trend that the capacitance of the Cs-137 exposed sample increases while the control decreases.

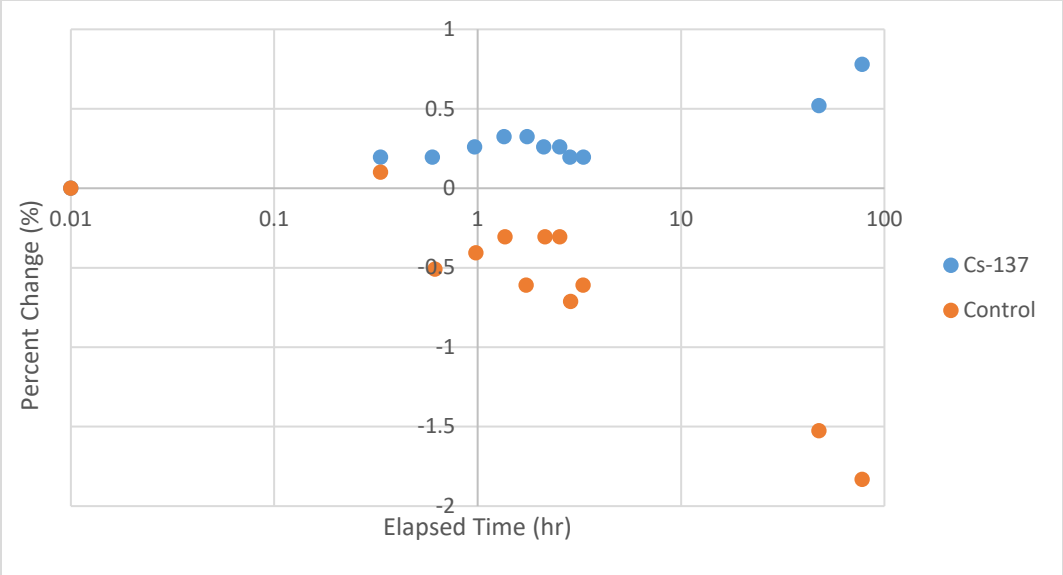

Figure 57. Iteration 4: Capacitance percent change (%) vs. elapsed time (hr)

Figure 58 shows the normalized values as a function of time.

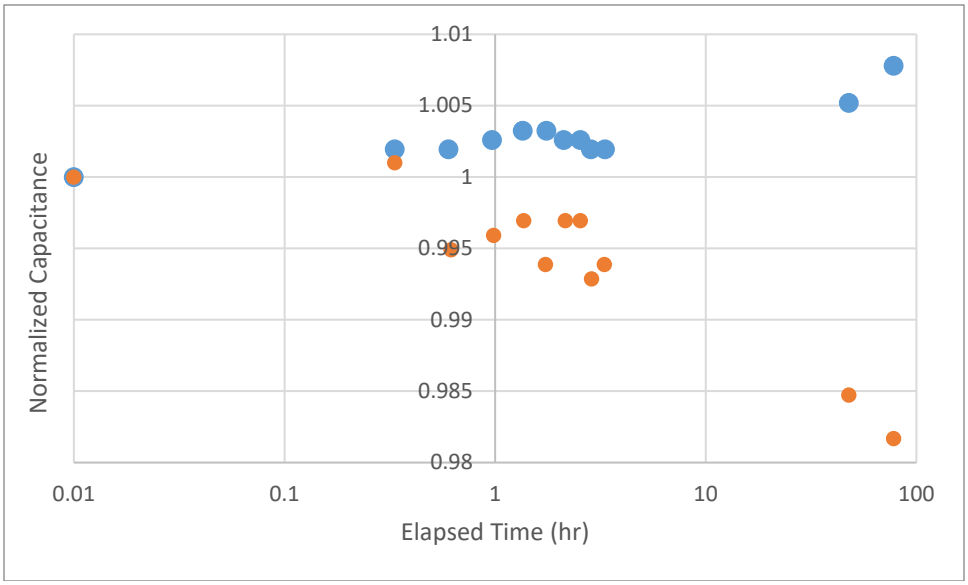

Figure 58. Iteration 4: Normalized capacitance vs. elapsed time (hr)

Figure 59 and Figure 60 show the difference in the normalized values. This serves as a way to determine if there is a difference between the Cs-137 exposed sample and the control. In this case, there is a significant difference indicating that the radiation had an effect on the dielectric.

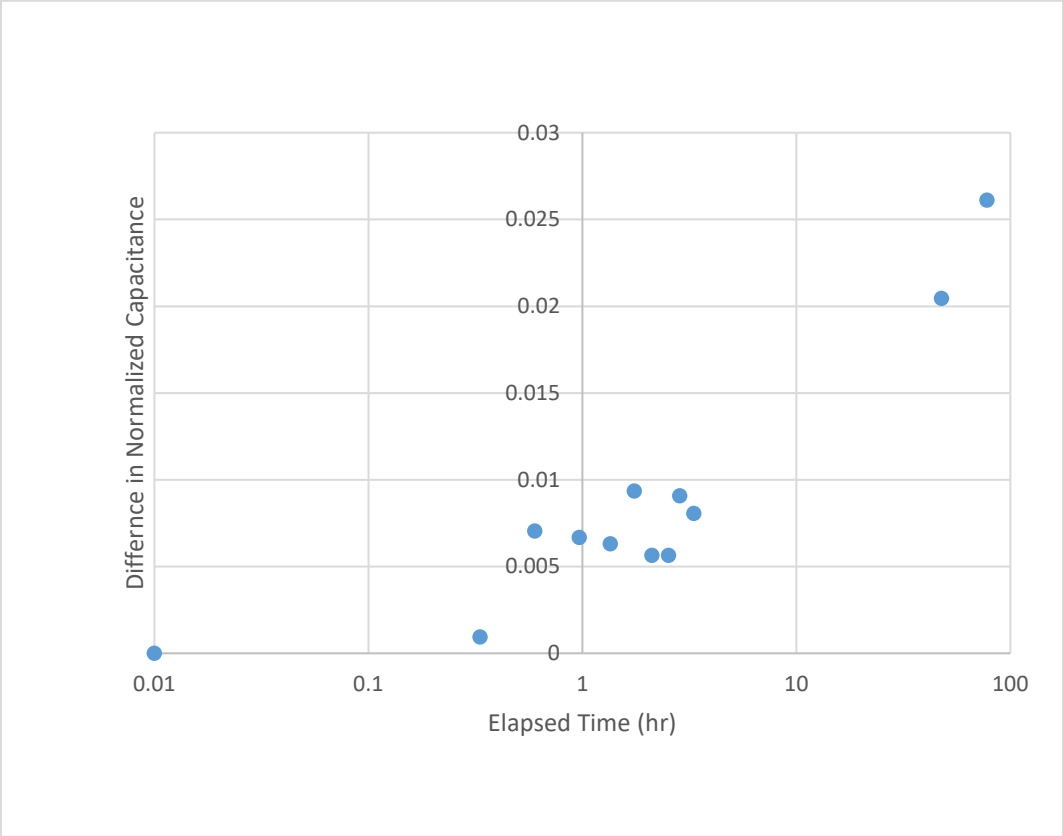

Figure 59. Iteration 4: Difference in normalized capacitance vs. elapsed time (hr)

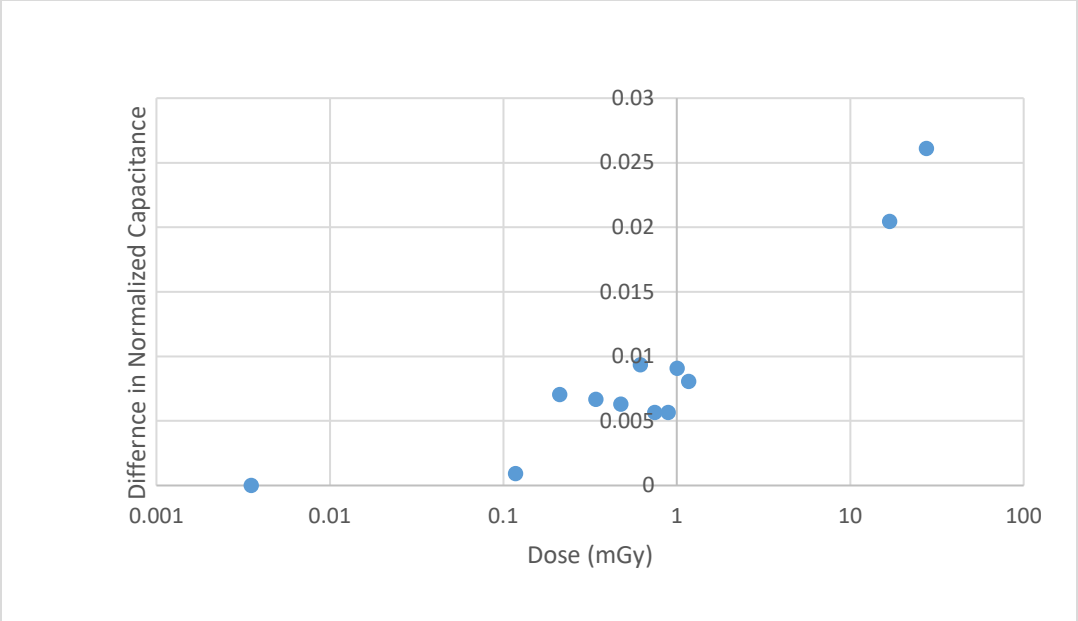

Dose only applies to irradiated sample

Figure 60. Iteration 4: Difference in normalized capacitance vs. dose (mGy)

Figure 61 shows the normalized capacitance as a function of humidity. The results indicate that there was no clear trend between the humidity and capacitance.

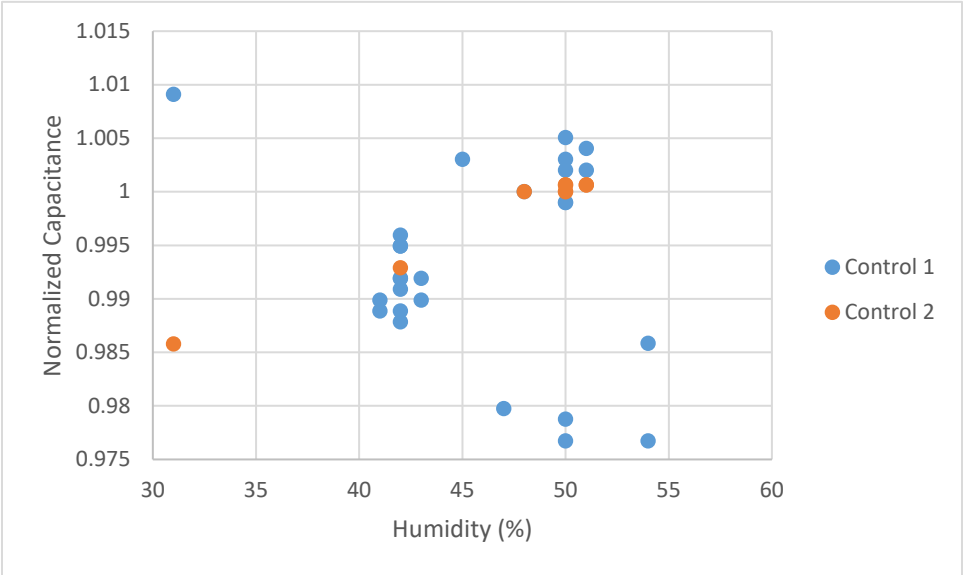

Figure 61. Iteration 4: Normalized capacitance vs. humidity (%)

Figure 62 shows the normalized capacitance as a function of temperature. The temperature remained mostly constant during the experiment at 70°F indicating that it had little effect on the capacitance change.

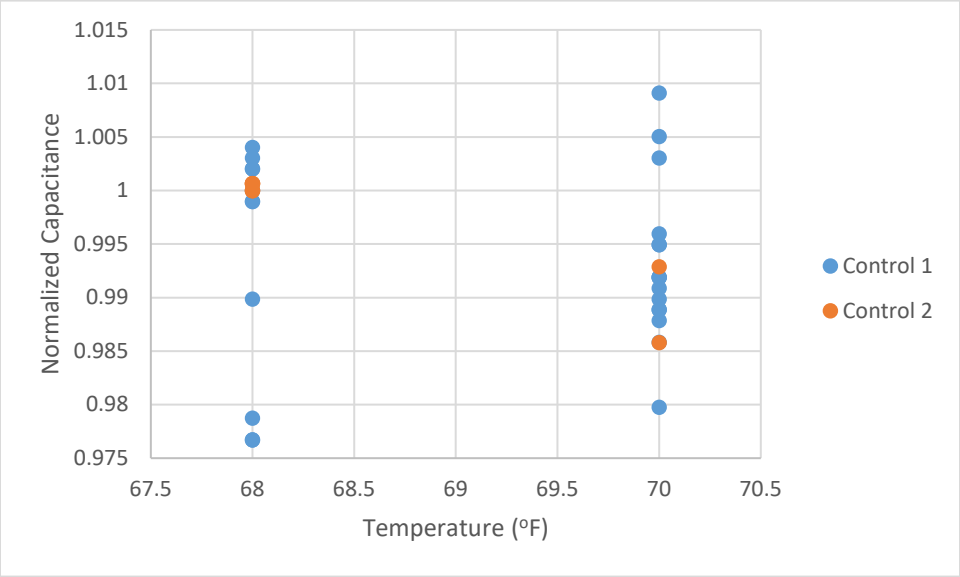

Figure 62. Iteration 4: Normalized capacitance vs. temperature (°F)

F. COMPARISON OF NORMALIZED VALUES

The normalized values serve as a way to compare standardized results from different experiments. The results from each iteration are shown in Figure 63 and Figure 64. Iteration 1, 3, and 4 show a positive difference in normalized values indicating that the Cs-137 exposed sample had a larger increase in capacitance as compared to the control. This indicates that the Cs-137 source did in fact change the molecular structure, and thus, the dielectric constant of the gamma-sensitive polymer. Iteration 2 was removed because there was likely an error in the experiment set up. Both capacitors were placed under lead shields but were not given time to reach equilibrium. Since the dielectric was still being compressed during the experiment, both capacitors show a net increase in capacitance and there could be no determination in whether the change in capacitance was a result of this compression or the radiation.

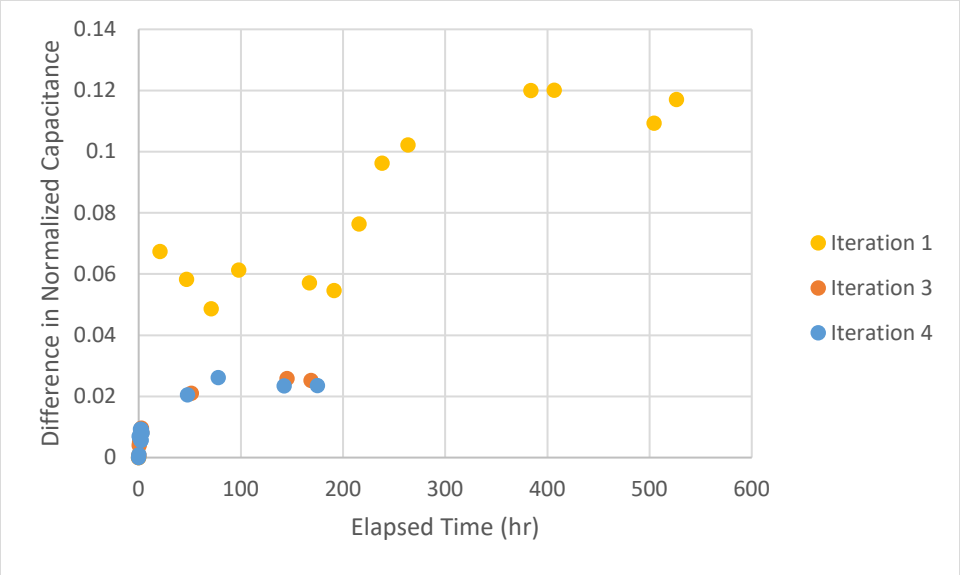

Figure 63. Difference in normalized capacitance vs. elapsed time (hr)

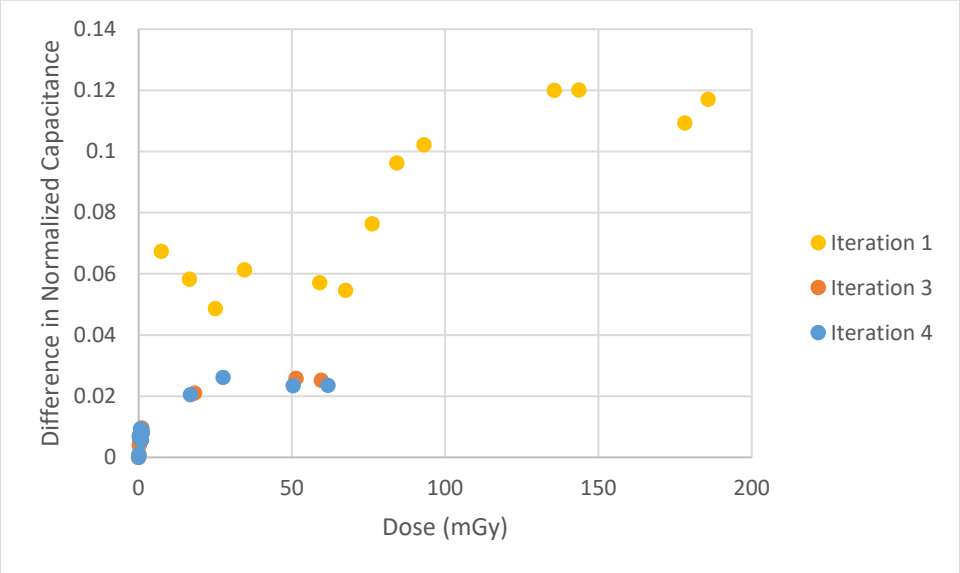

Dose only applies to irradiated sample

Figure 64. Difference in normalized capacitance vs. dose (mGy)

THIS PAGE INTENTIONALLY LEFT BLANK

IV. CONCLUSIONS AND FUTURE WORK

A. CONCLUSIONS FOR CAPACITIVE SENSOR

In conclusion, the PVDF dielectric does show an increase in relative dielectric constant ε_r when exposed to a Cs-137 source. This result was shown consistently in several iterations of experiments. However, the capacitors, as the ones used in the experiment, show a natural tendency to decrease in capacitance over time. This indicates that there are more factors at play in the capacitance changes than the radiation exposure. Out gassing of the dielectric, temperature, humidity, and light exposure all appear to have an effect on the capacitance. Additionally, this thesis established a standardized procedure for mixing and testing the dielectric. Several iterations were performed changing the wt % of the carbon black. It was found that 3 wt % carbon black worked best for the structural integrity of the dielectric. Furthermore, several experimental set ups were tested and it was concluded that placing both capacitors under a lead shield in the same environment yielded more consistent results by limiting the influence of external environmental factors.

B. FUTURE WORK FOR THE CAPACITIVE SENSOR

The results from this thesis do indicate that future work should be done with the PVDF dielectric. Environmental factors need to be explored to quantify its effect on the dielectric. These factors include light exposure, temperature, and humidity. Furthermore, the dielectric should be tested using terpinol-α rather than NMP as the solvent. The reference literature [4] used terpinol-α to conduct their experiments. For this thesis, terpinol-α was not available due to a delay in shipping. Thus, NMP was used as a substitute solvent. To have a true comparison with the reference literature terpinol-α must be used. The dielectric should be applied to a MEMS interdigitated sensor. This would ensure uniformity in both exposure and distance. The experiment set up in this thesis did not have uniform exposure and distance between the capacitors since the focus was determining whether PVDF was gamma-sensitive. The area of the Cs-137 source was smaller (0.0020268 m^2) compared to the area of the aluminum foil (0.00516 m^2). As a result, only a small fraction of the capacitor was exposed to the gamma radiation. Using a MEMS

interdigitated sensor would also allow comparison with the reference literature [4] as the capacitance would be on the pF scale. The gamma-sensitive capacitors can also be merged with the concept of super capacitors where the graphene electrodes can be used as one of the avenues to miniaturize and increase sensitivity.

APPENDIX A. COPPER PLATE CAPACITANCE DATA

Table 3. Copper plate capacitance data

Date/Time	Elapsed Time (hr)	Capacitance (nF)	Dose (mGy)
1/22/2020 13:54	0	1.415	0
1/23/2020 13:31	23.61666667	1.45	8.340331919
1/24/2020 13:30	47.6	1.32	16.81015382
1/27/2020 13:24	119.5	0.538	42.20196179
1/28/2020 11:07	141.2166667	0.49	49.87130018
1/29/2020 15:05	169.1833333	0.408	59.74785414
1/30/2020 12:36	190.7	0.392	67.34656162
2/3/2020 14:22	288.4666667	0.12	101.8732991
2/4/2020 12:47	310.8833333	0.096	109.7898457
2/5/2020 13:05	335.1833333	0.08	118.3714998
2/6/2020 10:47	356.8833333	0.106	126.0349523
2/10/2020 14:48	456.9	0.1034	161.3562874

THIS PAGE INTENTIONALLY LEFT BLANK

APPENDIX B. ITERATION 1 DATA

Table 4. Iteration 1: Cs-137 data

Date/Time	Elapsed Time (hr)	Capacitance (nF)	% Difference	Normalized	Dose (mGy)
2/24/2020 14:07	0	1.287	0	1	0
2/25/2020 11:00	20.88333333	1.385	7.614607615	1.076146076	7.375042975
2/26/2020 12:59	46.86666667	1.379	7.148407148	1.071484071	16.55117386
2/27/2020 12:59	70.86666667	1.359	5.594405594	1.055944056	25.02688167
2/28/2020 15:53	97.76666667	1.365	6.060606061	1.060606061	34.5267375
3/2/2020 13:18	167.1833333	1.301	1.087801088	1.010878011	59.04154515
3/3/2020 13:13	191.1	1.278	-0.699300699	0.993006993	67.48782342
3/4/2020 13:49	215.7	1.288	0.077700078	1.000777001	76.17542392
3/5/2020 12:28	238.35	1.306	1.476301476	1.014763015	84.17437317
3/6/2020 13:46	263.65	1.308	1.631701632	1.016317016	93.10918182
3/11/2020 14:03	383.9333333	1.296	0.699300699	1.006993007	135.5877813
3/12/2020 12:43	406.6	1.299	0.932400932	1.009324009	143.5926164
3/16/2020 14:34	504.45	1.269	-1.398601399	0.986013986	178.1487835
3/17/2020 12:19	526.2	1.245	-3.263403263	0.967365967	185.8298937

Table 5. Iteration 1: Control data

Date/Time	Elapsed Time (hr)	Capacitance (nF)	% Difference	Normalized	Dose (mGy)
2/24/2020 14:08	0	1.363	0	1	0
2/25/2020 10:56	20.8	1.375	0.880410858	1.008804109	7.345613434
2/26/2020 12:56	46.8	1.381	1.320616288	1.013206163	16.52763023
2/27/2020 12:48	70.66666667	1.373	0.733675715	1.007336757	24.95625077
2/28/2020 15:52	97.73333333	1.362	-0.073367572	0.999266324	34.51496568
3/2/2020 13:14	167.1	1.3	-4.622157007	0.95377843	59.01211561
3/3/2020 13:11	191.05	1.279	-6.162876009	0.93837124	67.4701657
3/4/2020 13:44	215.6	1.26	-7.556859868	0.924431401	76.14010848
3/5/2020 12:21	238.2166667	1.252	-8.14380044	0.918561996	84.1272859
3/6/2020 13:45	263.6166667	1.246	-8.584005869	0.914159941	93.09741
3/11/2020 14:01	383.8833333	1.209	-11.29860602	0.88701394	135.5701236
3/12/2020 12:39	406.5166667	1.212	-11.0785033	0.889214967	143.5631869
3/16/2020 14:28	504.3333333	1.195	-12.32575202	0.87674248	178.1075821
3/17/2020 12:14	526.1	1.159	-14.96698459	0.850330154	185.7945782

Table 6. Iteration 1: Normalized comparison

Cs-137	Control	Difference
1	1	0
1.076146	1.008804	0.067341968
1.071484	1.013206	0.058277909
1.055944	1.007337	0.048607299
1.060606	0.999266	0.061339736
1.010878	0.953778	0.057099581
0.993007	0.938371	0.054635753
1.000777	0.924431	0.076345599
1.014763	0.918562	0.096201019
1.016317	0.91416	0.102157075
1.006993	0.887014	0.119979067
1.009324	0.889215	0.120109042
0.986014	0.876742	0.109271506
0.967366	0.85033	0.117035813

THIS PAGE INTENTIONALLY LEFT BLANK

APPENDIX C. ITERATION 2 DATA

Table 7. Iteration 2: Cs-137 data

Date/Time	Elapsed Time (hr)	Capacitance (nF)	% Difference	Normalized	Dose (mGy)
3/17/2020 12:54	0	1.324	0	1	0
3/17/2020 13:17	0.383333333	1.332	0.604229607	1.006042296	0.135375889
3/17/2020 13:38	0.733333333	1.338	1.057401813	1.010574018	0.258979961
3/17/2020 14:05	1.183333333	1.343	1.435045317	1.014350453	0.417899482
3/17/2020 14:26	1.533333333	1.346	1.66163142	1.016616314	0.541503554
3/17/2020 14:48	1.9	1.348	1.812688822	1.018126888	0.670993535
3/19/2020 12:25	47.51666667	1.333	0.679758308	1.006797583	16.78072428
3/23/2020 13:38	144.7333333	1.341	1.283987915	1.012839879	51.11322681
3/24/2020 14:00	169.1	1.336	0.906344411	1.009063444	59.7184246
3/25/2020 14:34	193.6666667	1.333	0.679758308	1.006797583	68.39425328

Table 8. Iteration 2: Control data

Date/Time	Elapsed Time (hr)	Capacitance (nF)	% Difference	Normalized	Dose (mGy)
3/17/2020 12:55	0	1.162	0	1	0
3/17/2020 13:18	0.383333333	1.177	1.290877797	1.012908778	0.135375889
3/17/2020 13:38	0.716666667	1.18	1.549053356	1.015490534	0.253094053
3/17/2020 14:05	1.166666667	1.184	1.893287435	1.018932874	0.412013574
3/17/2020 14:27	1.533333333	1.188	2.237521515	1.022375215	0.541503554
3/17/2020 14:48	1.883333333	1.191	2.495697074	1.024956971	0.665107627
3/19/2020 12:26	47.51666667	1.222	5.163511188	1.051635112	16.78072428
3/23/2020 13:37	144.7	1.266	8.950086059	1.089500861	51.10145499
3/24/2020 14:00	169.0833333	1.27	9.294320138	1.092943201	59.71253869
3/25/2020 14:34	193.65	1.281	10.24096386	1.102409639	68.38836738

Table 9. Iteration 2: Normalized comparison

Cs-137	Control	Difference
1	1	0
1.006042	1.012909	-0.00686648
1.010574	1.015491	-0.00491652
1.01435	1.018933	-0.00458242
1.016616	1.022375	-0.0057589
1.018127	1.024957	-0.00683008
1.006798	1.051635	-0.04483753
1.01284	1.089501	-0.07666098
1.009063	1.092943	-0.08387976
1.006798	1.10241	-0.09561206

THIS PAGE INTENTIONALLY LEFT BLANK

APPENDIX D. ITERATION 3 DATA

Table 10. Iteration 3: Cs-137 data

Date/Time	Elapsed Time (hr)	Capacitance (nF)	% Difference	Normalized	Dose (mGy)
4/15/2020 10:59	0	1.143	0	1	0
4/15/2020 11:14	0.25	1.144	0.087489064	1.000874891	0.088288623
4/15/2020 11:33	0.566666667	1.144	0.087489064	1.000874891	0.200120879
4/15/2020 11:51	0.866666667	1.144	0.087489064	1.000874891	0.306067226
4/15/2020 12:08	1.15	1.145	0.174978128	1.001749781	0.406127666
4/15/2020 12:28	1.483333333	1.145	0.174978128	1.001749781	0.52384583
4/15/2020 13:03	2.066666667	1.145	0.174978128	1.001749781	0.729852617
4/15/2020 13:44	2.75	1.146	0.262467192	1.002624672	0.971174853
4/15/2020 14:04	3.083333333	1.147	0.349956255	1.003499563	1.088893017
4/17/2020 14:36	51.61666667	1.159	1.399825022	1.01399825	18.2286577
4/21/2020	145.2166667	1.152	0.787401575	1.007874016	51.28391815
4/22/2020	168.6333333	1.162	1.662292213	1.016622922	59.55361917

Table 11. Iteration 3: Control data

Date/Time	Elapsed Time (hr)	Capacitance (nF)	% Difference	Normalized	Dose (mGy)
4/15/2020 11:00	0	1.282	0	1	0
4/15/2020 11:16	0.266666667	1.282	0	1	0.094174531
4/15/2020 11:33	0.55	1.278	-0.31201248	0.996879875	0.194234971
4/15/2020 11:51	0.85	1.277	-0.390015601	0.996099844	0.300181318
4/15/2020 12:09	1.15	1.277	-0.390015601	0.996099844	0.406127666
4/15/2020 12:27	1.45	1.276	-0.468018721	0.995319813	0.512074013
4/15/2020 13:03	2.05	1.274	-0.624024961	0.99375975	0.723966709
4/15/2020 13:44	2.733333333	1.273	-0.702028081	0.992979719	0.965288945
4/15/2020 14:04	3.066666667	1.276	-0.468018721	0.995319813	1.083007109
4/17/2020 14:36	51.6	1.273	-0.702028081	0.992979719	18.22277179
4/21/2020 12:12	145.2	1.259	-1.794071763	0.982059282	51.27803224
4/22/2020 11:38	168.6333333	1.271	-0.858034321	0.991419657	59.55361917

Table 12. Iteration 3: Normalized comparison

Cs-137	Control	Difference
1	1	0
1.000875	1	0.000874891
1.000875	0.99688	0.003995015
1.000875	0.9961	0.004775047
1.00175	0.9961	0.005649937
1.00175	0.99532	0.006429968
1.00175	0.99376	0.007990031
1.002625	0.99298	0.009644953
1.0035	0.99532	0.00817975
1.013998	0.99298	0.021018531
1.007874	0.982059	0.025814733
1.016623	0.99142	0.025203265

THIS PAGE INTENTIONALLY LEFT BLANK

APPENDIX E. ITERATION 4 DATA

Table 13. Iteration 4: Control comparison data

Date/ Time	Elapsed Time (hr)	Capacitance (nF)	% Difference	Normalized	Capacitance (nF)	% Difference	Normalized	Temperature (F)	Humidity (%)	Difference in Normalized
4/29/ 2020 11:06	0	0.988	0	1	1.549	0	1	68	48	0
4/29/ 2020 11:31	0.416666667	0.987	-0.101214575	0.998987854	1.549	0	1	68	50	-0.001012146
4/29/ 2020 11:56	0.833333333	0.987	-0.101214575	0.998987854	1.549	0	1	68	50	-0.001012146
4/29/ 2020 12:27	1.35	0.99	0.202429 15	1.002024291	1.55	0.064557779	1.000645578	68	50	0.001378714
4/29/ 2020 12:57	1.85	0.991	0.303643725	1.003036437	1.55	0.064557779	1.000645578	68	50	0.002390859
4/29/ 2020 13:21	2.25	0.99	0.202429 15	1.002024291	1.55	0.064557779	1.000645578	68	51	0.001378714
4/29/ 2020 13:45	2.65	0.992	0.404858 3	1.004048583	1.55	0.064557779	1.000645578	68	51	0.003403005
5/ 1/2020 14:32	51.43333333	0.997	0.910931174	1.009109312	1.527	-1.420271143	0.985797289	70	31	0.023312023
5/ 6/2020 10:28	167.3666667	0.983	-0.506072874	0.994939271	1.538	-0.710135571	0.992898644	70	42	0.002040627

THIS PAGE INTENTIONALLY LEFT BLANK

LIST OF REFERENCES

[1] World Health Organization, “Ionizing radiation, health effects and protective measures,” WHO, April 29, 2016. [Online]. Available: https://www.who.int/news-room/fact-sheets/detail/ionizing-radiation-health-effects-and-protective-measures

[2] F. N. Flakus, “Detecting and measuring ionizing radiation—A short history,” *IAEA Bull*., vol. 23, no. 4, p. 6.

[3] Glenn F. Knoll, *Radiation Detection and Measurement*. Hoboken, NJ, USA: John Wiley & Sons, Inc., 2000.

[4] O. Korostynska, K. Arshak, D. Morris, A. Arshak, and E. Jafer, “Radiation-induced changes in the electrical properties of carbon filled PVDF thick films,” *Mater. Sci. Eng. B*, vol. 141, no. 3, pp. 115–120, Aug. 2007, doi: 10.1016/j.mseb.2007.06.025

[5] B. Seitz, N. C. Rivera, R. Gray, A. Powell, and F. Thomson, “Radiation sensors for medical, industrial and environmental applications: How to engage with schools and the general public,” *Phys. Educ.*, vol. 53, no. 1, p. 014001, Nov. 2017, doi: 10.1088/1361-6552/aa9056

[6] A. Goel, “Thermoluminescent dosimeter,” Radiopaedia, accessed April 19, 2020, https://radiopaedia.org/articles/thermoluminescent-dosimeter?lang=

[7] R. L. Murray, “Radiation detectors: Suggestions by Glenn F. Knoll are recognized with appreciation,” in *Nuclear Energy (Sixth Edition)*, R. L. Murray, ed. Boston, MA, USA: Butterworth-Heinemann, 2009, pp. 125–140.

[8] *An Introduction to MEMS (Micro-electromechanical Systems)*. Loughborough, England: PRIME Faraday Partnership, 2002.

[9] S. Cheriyedath, “What is Lab-on-a-Chip?,” News-Medical.net, Feb. 14, 2020. [Online]. Available: https://www.azolifesciences.com/article/What-is-Lab-on-a-Chip.aspx

[10] Nuclear Regulatory Commission, “NRC: Radiation basics.” Accessed April 19, 2020. [Online]. Available: https://www.nrc.gov/about-nrc/radiation/health-effects/radiation-basics.html

[11] ResearchGate, “Figure 3.10: Sketch of photoelectric absorption process.” Accessed April 19, 2020. [Online]. Available: https://www.researchgate.net/figure/Sketch-of-photoelectric-absorption-process_fig17_254468999

[12] D. J. Griffiths, *Introduction to Electrodynamics*, Fourth edition. Boston, MA, USA: Pearson, 2013.

[13] C.R. Nave, “Polarization of dielectric,” Hyperphysics. Accessed April 19, 2020. [Online]. Available: http://hyperphysics.phy-astr.gsu.edu/hbase/electric/dielec.html

[14] G. Ribeiro, H. A. Zen, A. N. Geraldes, C. P. Souza, and D. F. Parra, “Gamma irradiation effects on poly(vinylidene fluoride) films,” presented at the 2009 Int. Nuclear Atl. Conf., Rio de Janeiro, RJ, Brazil, Sept. 7, 2009.

[15] Omnexus, “Polyvinylidene Fluoride (PVDF) Plastic: Material Properties & Other Info.” Accessed April 19, 2020. [Online]. Available: https://omnexus.specialchem.com/selection-guide/polyvinylidene-fluoride-pvdf-plastic

[16] Z. Hameed and J. V. Gats, “Boron-nitride nanotubes and versatile dielectrics for MEMS electronic nose radiation detector,” M.S. thesis, Dept. of Physics, NPS, Monterey, CA, USA, 2019. [Online]. Available: http://hdl.handle.net/10945/62807.

[17] Calculator.org., “Solid angle.” Accessed April 19, 2020. [Online]. Available: https://www.calculator.org/properties/solid_angle.html

[18] jwmillerFollow, “Aluminum foil plate capacitor,” Instructables. Accessed April 19, 2020. [Online]. Available: https://www.instructables.com/id/Aluminum-Foil-Plate-Capacitor/

INITIAL DISTRIBUTION LIST

1. Defense Technical Information Center
   Ft. Belvoir, Virginia

2. Dudley Knox Library
   Naval Postgraduate School
   Monterey, California